LOCATING AMAZONIAN DARK EARTHS (ADE) IN THE BRAZILIAN AMAZON USING SATELLITE IMAGERY

By

Jonathan B. Thayn

Submitted to the graduate degree program in
Geography and the Graduate Faculty of the
University of Kansas in partial fulfillment of the
requirements for the degree of Doctor of Philosophy

_____

Co-Chairperson

_____

Co-Chairperson

_____

_____

_____

Date Defended _____

The Dissertation Committee of Jonathan Boyd Thayn certifies that this is the approved version of the following dissertation:

LOCATING AMAZONIAN DARK EARTHS (ADE) IN THE BRAZILIAN AMAZON USING SATELLITE IMAGERY

Committee:

_____
Co-Chairperson

_____
Co-Chairperson

_____

_____

_____

Date Approved _____

Abstract

Amazonian Dark Earths (ADE) are patches of archaeological soils scattered throughout the Amazon Basin. These soils are anthropogenic and most evidence suggests that they are the result of unintentional cultural deposits as well as intentional efforts of Amerindian populations to improve the quality of their farmlands. ADE are a mixture of charcoal, organic matter and the underlying Oxisol soil. ADE are extremely fertile soils in comparison to the surrounding Oxisols and they are sought after by local residents for agricultural purposes. In the first chapter I discuss the value and physical properties of ADE in detail. Research is being conducted to learn how ADE were created and to explore the possibility of replicating them to sequester carbon and to reclaim depleted soils in the Amazon Basin. This dissertation seeks to assist in that effort by attempting to map currently unknown ADE sites hidden beneath the dense tropical forest canopy.

Brazilian archaeologists who accompanied surveyors plotting the route of a future natural gas pipeline discovered 28 previously unknown ADE sites. These sites have been untouched since their abandonment centuries ago. This data-set allows me to examine the effects of ADE soil on the forest canopy using satellite imagery collected before gas pipeline construction began in 2006. I used annual time-series of Moderate Resolution Imaging Spectroradiometer (MODIS) Enhanced Vegetation Index (EVI) satellite imagery from 2001 through 2005. EVI data estimate the amount of green, or photosynthetically active, vegetation in each pixel of the satellite image. I used a combination of descriptive statistics, Harmonic Wave Analysis (Fourier Transform) variables, MANOVA tests and logistic regressions to attempt to locate ADE sites using the differences in EVI values as a surrogate for soil type.

In chapter 2 I discuss the application of harmonic wave analysis and presents the underlying theory that justifies its use. In chapter 3 I deal with the application of the methodology to the gas pipeline data. While some differences were apparent between the two soil types, the distribution of EVI values for both soil types were too broad for an accurate image classification. Although an accurate map was not possible, this research did demonstrate that the methodology has real potential and may be successful when applied to a time-series with higher spatial resolution. This research also demonstrates that harmonic phase angles can be interpreted to represent phenologic variation in tropical forest vegetation. Phase angles are less intuitive than other methods for estimating phenology, but the method is much more robust in regions with slight seasonal variation, such as the tropics. In chapter 4 I discuss directions for future research and some of the tangential projects that have grown from this study.

To Debbi, who said,
“You’re not happy. I think you
Should go back to graduate school.”
For that, and everything else,
I will love you through eternity.

Acknowledgements

I am indebted to the following people for sharing their wisdom and their time.

Kevin Price, whose support (intellectual, emotional and spiritual) made this whole process easier. Kevin is an approachable teacher and a good friend. I decided to come to the University of Kansas so that I could work with Kevin, and I absolutely made the right decision. Also, to his grandparents who bought eggs and milk from my grandparents and whose friendship made living on far-flung arid farms a little more enjoyable.

Bill Woods, whose instruction, friendship and financial support made traveling to Brazil possible and fun. Also for introducing me to Panama, a beautiful country to which I will return.

Steve Egbert, an excellent teacher and a good man. My goal is to teach class as well as you do. I appreciate your patience.

Steve Bozarth who served on my committee and suggested that indicator species may be the key to mapping Amazonian Dark Earths. I should have listened the first time.

Bryan Foster who ensured that my research was up to par.

Wenceslau Teixeira, who tirelessly returned my emails and provided a lot of information. I hope we continue to work together for a long time.

Gilvan Martins, who helped me in Manaus and who taught me funny words like Tucupi, Tipití and Tacacá.

Eduardo Neves, and his archaeology students, for allowing me to participate in the 2007 Archaeology Field School. They very patiently taught me how excavate and clean ceramic shards, answered my questions, and gave me copies of their reports and data. This project would have been more difficult and less fun without them.

Newton Falção, for tirelessly applying science to making the life of subsistence farmers easier and for showing me his experiments at the “fruit salad”.

Jude Kastens, who understands math and can patiently explain it.

Chris Brown and Wendy Jepson who allowed me to follow them around Vilhena, Rondonia, Brazil asking questions about geographic methods and Portuguese pronunciation.

André Junquiera for sharing his data and for extending an offer of friendship and future collaboration. I am excited to work with you in the future.

Dovis Pollock, whose Portuguese instruction made my second visit to Brazil much easier.

All of the professors and staff of the Department of Geography and the Kansas Applied Remote Sensing (KARS) program at the University of Kansas. You have made this a wonderful experience.

The American Society for Photogrammetry and Remote Sensing (ASPRS), the ASPRS Central Region, the Kansas Academy of Science and the Center for Latin American Studies at KU for their financial support.

Above all of these, I am grateful for my parents, Boyd and Mary Thayn, who taught me the true importance of family and avocation; and for my children, Mary, Lucy, Henry and Ben, who reminded me how to play “stuffed animal veterinarian” and who never seem to get tired of penguin jokes; and for my wife, who works harder than I do and kisses me every day.

Table of Contents

List of Figures

List of Tables

Chapter 3: Applications of Methodology

Figure i.i A map of the general area

Chapter 1

An Introduction to Amazonian Dark Earths

1.1 Introduction

Soil is the largest pool of organic carbon in the global biosphere—most soils contain more carbon than is present in the vegetation growing in them (Jobbágy and Jackson 2000). This is not true of tropical forests which, although they occupy 16.7 percent of the earth's surface, contain only 6.5 percent of the world's soil organic matter (SOM) and a whopping 42.2 and 55.6 percent of the planet's total net primary production and total plant biomass (measured in metric tons of carbon), respectively (Schlesinger 1991). Because of topical climatic conditions in the Amazon Basin, nutrient cycles occur on a thin superficial horizon that rests on the soil, rather than within the soil itself, making typical Amazonian soils chemically poor and infertile (Sombroek 1966).

Amazonian Dark Earths (ADE) are an exception. These soils are anthropogenic, the result of prehistoric human occupation (Neves et al. 2003), and contain elevated levels of nutrients that make them very fertile (Kern et al. 2003; Lehmann et al. 2003a; Lehmann et al. 2003b). Major *et al.* (2005) report that maize yields in plots of ADE are as much as 63 times greater, weed ground cover is 45 times greater, species richness is up to 11 times greater, and the total number and variety of seedlings are

greater than in adjacent soils. These soils contain up to 70 times more SOM than typical Amazonian soils (Mann 2002).

ADE soils, which were typical low-fertility soils before prehistoric human influence, offer a unique opportunity to study the feasibility of using carefully managed habitation and agricultural sites within the Amazon Basin for carbon sequestration (Glaser et al. 2003b; Marris 2006; Sombroek et al. 2002). This process, which would involve increasing the SOM and nutrient levels in soils, would restore depleted land (Sombroek 1966) and limit the need for clearing additional land (for a contrary view see Meggers 2001). Despite occurring frequently, individual ADE patches are too small (80% of known ADE sites are smaller than 2 hectares - Kern et al. 2003) to appear on most soil surveys (Glaser et al. 2001 316; McCann et al. 2001; Sombroek et al. 2002). While some rudimentary maps exist (Heckenberger et al. 1999), the geographic extent and location of ADE soils are largely unknown (Woods 1995) and comprehensive ground surveys under the extremely difficult field conditions are infeasible for even a small portion of the enormous region.

Most known ADE sites have been found by local small-holder and subsistence farmers who prefer ADE soils because of its heightened fertility (Sombroek et al. 2002). Woods and McCann (1999) report that local residents recognize ADE soils based on their lower vegetation canopy and more closed understory, and unique species compositions.

Traditional ground-based field methods are unsuited for locating ADE soils because of the logistical difficulties associated with fieldwork in the dense, inaccessible tropical forest. Also, the time and financial cost that would be required to search the enormous extent of the Amazon Basin in prohibitive. Methods for predicting the location of ADE are required. Such information would greatly enhance researcher's ability to find new sites, could contribute to preserving tropical forests in the region, and would assist scientists' efforts to study and replicate ADE soils in support of a carbon sequestration industry.

1.2 History

In 1542 Francisco de Orellana (a cousin of Pizarro who had conquered Peru just nine years earlier) and his crew of 60 became the first Europeans to navigate the Amazon River (Fig. 1.1). They wrote to Spain of "very large settlements," with each village no more than a "crossbow shot" from the next. They spoke of a single Amerindian community that stretched along the riverbank for 15 miles and "very fine" highways that extended at least six miles into the interior and terminated in large cites that "glistened white" in the distance (Woods 2002, Mann 2002). Many times, the riverbanks bristled with armed warriors and the explorers were harassed by flotillas of huge war-canoes (Carvajal 1934, Smith 1994).

Later explorers, however, found no evidence of large indigenous populations. In fact, many scientists have suggested that Amerindian settlements of the size de-

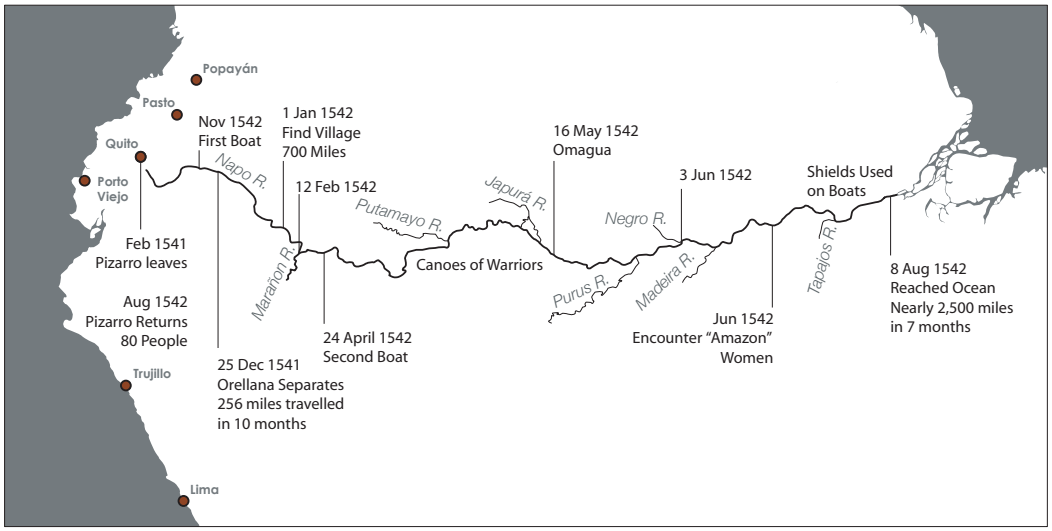

Figure 1.1 Orellana's voyage of discovery down the Amazon River. The expedition's scribe, Friar Gaspar de Carvajal, recorded many large population centers along the river's course; however, the damage done to Orellana's reputation by the subsequent treason trial, the claim of encountering tribes led by "Amazon" women, and a lack of further expeditions conspired to throw Carvajal's account into disrepute. Source: Smith 1994.

scribed by Orellana are impossible in the Amazon Basin due to the agriculture-limiting nutrient-poor Oxisol soils that dominate the region. Betty Meggers (1992; 199), the principal of these scientists, has stated that there is "no evidence that … communities were larger, more closely spaced or more sedentary in pre-Columbian times than indigenous communities today." She suggests that the pattern of small, dispersed, semi-nomadic communities that exist in this century has "existed for at least two millennia without significant alteration in village size or permanence" (Meggers et al. 1988; 291). This theory has permeated modern thinking so that the Amazon Basin is largely envisioned as pristine untouched forest.

The recent discovery of ADE, known locally as *terra preta do Índio* or "dark earth of the Indians," may provide evidence that challenges the current paradigm and

corroborate Orellana's historical account. These soils suggest that the Amazon Forest is, at least in part, a manipulated forest rather than an untouched forest (Mann 2005: 300-311). In addition to having approximately twice the amount of soil organic matter (SOM) and higher mineral concentrations than is present in typical Amazonian soils (Woods and McCann, 1999; Sombroek et al. 2002), ADE also contain dense concentrations of pottery sherds and other ceramic artifacts (Fig. 1.2 and 1.3 - Neves et al. 2003; Sombroek 1966). ADE soils derive their dark coloration from the addition of charcoal to the underlying soil (Glaser et al. 2003b; Lehmann 2007). Modern smallholder farmers continue the practice of charing vegetation and mixing the charcoal and ash into the soil as a means of stabilizing soil nutrient levels (Fig. 1.4).

In addition to opening a window to the past, these soils may offer a key to the future. The most readily observed characteristic of ADE soils is their high concentration of charcoal. Glaser et al. (2003b) found 64 times more charcoal in ADE soils than in the surrounding soils, although four times more charcoal is more typical (Glaser et al. 2001). To meet the challenges of possible global climate change caused by greenhouse gas emissions, atmospheric carbon concentrations must be reduced and the carbon sequestered in a stable pool. Charcoal, or biochar, is created when organic matter is heated without oxygen and it contains twice the carbon content of ordinary biomass (Lehmann 2007). Charcoal is much more resistant to decay and can lock away carbon for millennial timescales (Lehmann et al. 2006). The addition of charcoal to the soil was part of the creation of ADE (Neves et al. 2003). This has led some

Figure 1.2 Examples of three trenches excavated at Laguinho in 2007. Notice the dense concentrations of ceramic sherds in the soil. It is possible to see the different colors of the orange Oxisols and the brown-to-black Amazonian Dark Earths (ADE).

Figure 1.3 Ceramic sherds collected at Laguinho during the archaeological expedition of 2007.

to speculate on the viability of a biochar carbon sequestration industry which would reduce atmospheric greenhouse gases and retard possible CO_2 induced climate change (Lehmann 2007; Lehmann et al. 2006; Marris 2006; Sombroek et al. 2002). This industry would also improve soil fertility (Fig. 1.5, Lehmann et al. 2003a) and could reduce the need for deforestation for farmland.

ADE soils were first thought to be derived from the accretion of cultural waste around inhabited areas; however, only a portion of known ADE sites show evidence of long-term human habitation (Woods et al. 2000). Other findings, including the association of ADE soils with structural features like burial mounds, artifact distributions, and the lack of intervening non-cultural sediments, suggest that these modified soils are the intentional result of large, permanent prehistoric communities working to

Figure 1.4 Modern primitive charcoal production sites. The first photograph is a log kiln where whole trees are buried and then burned with low levels of oxygen. The resulting charcoal is then mixed with soils in home garden plots and subsistence farms. We were able to find several of these trough-style kilns at the same farm. Apparently, the landowner builds a new one at the site of his most recently cleared field site. The area in the background of this photograph served as the source of the trees for this kiln. Undoubtedly this newly cleared site will become his next field. The second photograph is a clay charcoal kiln. Wood is placed inside and ignited and then the doorway is sealed to prevent the entry of oxygen. This charcoal is then sold to families who use it for cooking.

improve the quality of their farmlands (Heckenberger, 1999). Indeed, the current inhabitants of the Amazon Basin prize ADE soils for their heightened fertility (Fig. 1.6, Woods 1995). These soils have been fertile for at least 2,000 years, making them capable of sustaining population centers (Mann 2005).

Figure 1.5 EMBRAPA field station research efforts. The Brazilian Agricultural Research Agency (EMBRAPA) is investing many resources into creating new Amazonian Dark Earths (ADE) and determining the effects of ADE soils on crop yields. The first photograph is of an açai field (a dark, fruity berry related to chocolate) where charcoal is routinely added to the soil. The second photograph is of a similar experiment involving bananas. The açai and banana experiments are being conducted by Wenceslau Teixeira (in the yellow shirt). The third photograph is an experiment involving rice and grains being conducted by Newton Falcõa (in the red shirt).

Figure 1.6 The archaeological site at Laguinho, near Iranduba, Brazil. The field study group from the University of São Paulo excavated this site during the 2007 archaeological season. The site is located on an active papaya plantation.

1.3 Origins

Large ADE sites on the plateau south of Santarem were reported in the 1870's (see Woods and Denevan, 2009: 3-10 for a detailed discussion of early reports). Later, Steere (1927) wrote of these ADE patches while visiting the plantations of expatriate Confederate land owners who had fled to Brazil after the U.S. Civil War. Once a contentious issue (Woods 2003), it is now generally accepted that ADE soils are the result of past human activity, either intentional or incident to prolonged habitation.

There are two types of ADE: *terra preta* (black earth) which are defined by a darker brown or black color, the presence of pottery sherds (Fig. 1.2 and 1.3), and drastically increased concentrations of charcoal or pyrogenic carbon within the A horizon; and *terra mulata* (brown earth) characterized by the absence of pottery sherds or other artifacts, and lower levels of soil organic matter (SOM) and charcoal (Neves et al. 2003, Woods and McCann 1999). The presence of pottery shards and higher concentrations of charcoal in the *terra preta* soils could be the result of cooking fires and trash discard areas (Heckenberger et al. 1999). The *terra mulata* sites, however, cannot be explained by this theory. These soils are generally found near the periphery of *terra preta* sites and have almost no artifact inclusions. *Terra mulata* soils contain similar amounts of organic carbon to *terra preta,* but with lower available phosphorus and calcium contents (Woods and McCann 1999), which is contrary to what is expected if these sites were trash discard areas (McCann et al. 2001). This suggests that the formation of *terra mulata* sites was the result of intentional efforts of prehistoric

Amerindian populations to improve the quality of their farmland (Neves et al. 2003, Woods and McCann 1999). Neves (2003) has shown that nutrient transfers from outside of the cropped areas were necessary to explain the nutrient levels observed today. These nutrient sources may have been food wastes, fish bones and other unused fish matter or human excrement. The presence of algae in ADE in Colombia from c.a. 1,150 BP and later suggests that silt from riverbanks was incorporated into the agricultural areas in at least one location (Mora et al. 1991).

The earliest evidence of human habitation in the Amazon basin has been found in caves near Santarém and dates to 11,000-10,000 BP (Roosevelt et al. 1996). The discovery of semi-polished stone axes in the Amazon basin indicates that some form of forest manipulation began as early as 8,000 BP (Neves et al. 2003; Oliver 2001), although large-scale clearing was limited by the difficulty of cutting trees with stone (Denevan 1992). It is likely that natural plant distributions were managed beginning around this time. Human management of useful trees and plants created patches or "orchards" of semi-domesticated species such as the açai palm (*Euterpe oleracae Mart*.) and Brazil nut (*Bertholletia excelsa Humb*. and *Bonpl*.). These orchards are scattered throughout Amazonia (Neves et al. 2003). Heckenberger *et al.* (2003) report that prehistoric settlements had substantial influence on the landspace, including acute forest alteration and secondary forest growth sites (containing tree species whose distributions are generally restricted to ADE soils) that were clearly visible in satellite imagery. It is still common practice among indigenous groups to

nurture and enlarge concentrations of useful tree species. These sites are often called drought gardens or emergency gardens and are passed through the family line (Lukesch 1976).

The oldest ADE soils are 2,500 years old and they can be as young as 500 years old (Neves et al. 2003). Neves et al. (2003) suggested that the formation of ADE is more strongly correlated to population density than to duration of habitation and that formation of ADE was more rapid than previously thought. This implies that, by some mechanism, the human population in the Amazon basin experienced a surge at approximately 2,500 B.P. Additional anthropologic research is necessary to validate this assumption.

1.4 Distribution

ADE soils are present in nearly all the eco-regions of the Amazon basin (Kern et al. 2003). They are found principally in the Brazilian Amazon, where it has been estimated that there is a *Terra Preta* patch for every 2 km^2 along certain rivers, but they extend into Colombia, Venezuela, Peru, Bolivia and the Guianas as well (Sombroek et al. 2002). ADE soils are not limited to river corridors. Forty-five percent of archaeological sites are between 5 and 25 m above water sources, and more than half are located far from water sources (Kern et al. 2003). They are found on a variety of soil types, including Ferrasols, Podzols, Acrisols, Luvisols, Fluvisols, Nitrisols, Cambisols, and Arenasols (Kern et al. 2003). Several maps of ADE distributions have

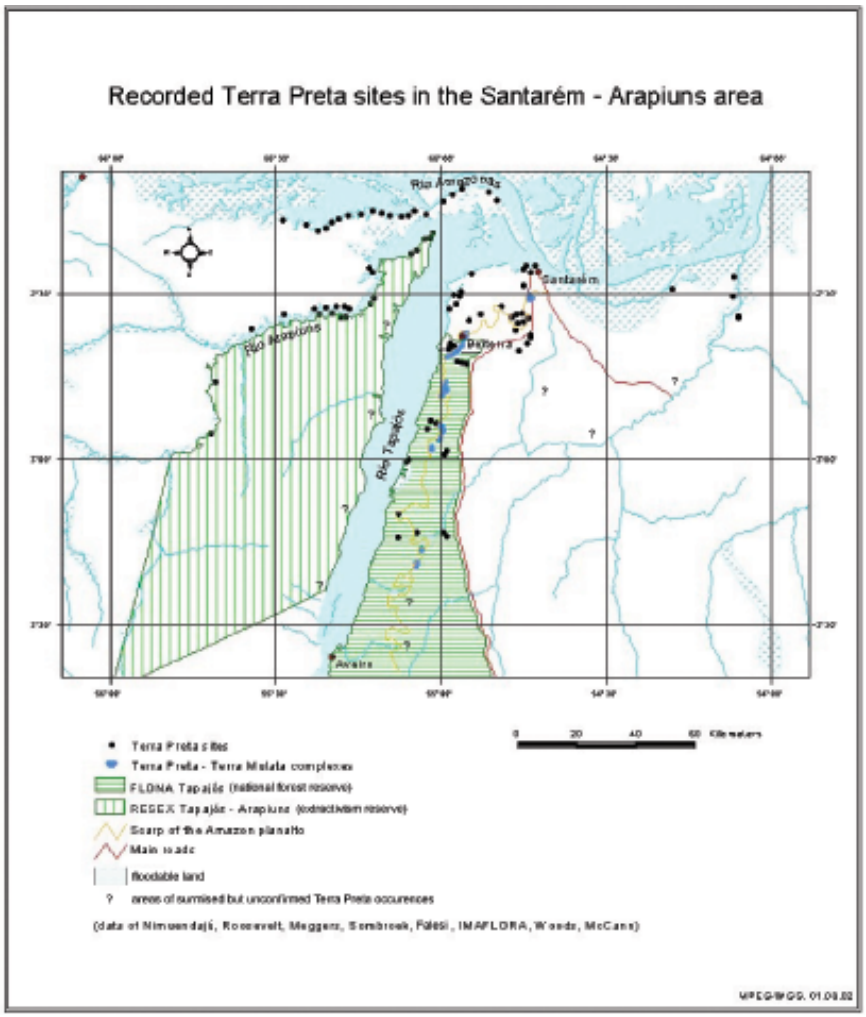

Figure 1.7 Map of Amazonian Dark Earth sites near Santarém, Brazil. This map was prepared by Wim Sombroek and William Woods and is one of the most detailed in existence.

been published (Heckenberger et al. 1999; Kern et al. 2003), although these maps can be considered incomplete at best (Fig. 1.7). There are no ADE maps of the entire Amazon Basin, and all current maps indicate only those sites that have been reported by professional researchers. This dissertation attempts to more accurately map ADE distribution using satellite imagery.

1.5 Physical Characteristics

ADE soils are defined by the presence of a diagnostic plaggic, terric or hortic A horizon (Teixeira and Martins 2003). Plaggic strata contain large concentrations of organic carbon; terric horizons are anthropogenic and develop through the addition of earthy manures, compost or mud; and hortic soils result from deep cultivation, intensive fertilization and/or long-continued application of human and animal wastes. The A horizon of ADE soils typically have a depth of 30 to 60 cm, characterized by brown to black color (5YR 2/1, 7.5YR 3/1, to 10YR 3/1 - Kern et al. 2003: 68), while surrounding A horizons are only 10 to 15 cm thick (Fig. 1.8). The dark coloration is caused by melanization with organic material and black carbon (Glaser et al. 2003a). Organic matter is concentrated in the upper 20 cm of the soil with a high amount of exchangeable aluminum (pH 4.5 or lower) (Kern et al. 2003). In general, ADE soils have higher pH, higher cation exchange capacity, higher base saturation, and higher nutrient levels than do the surrounding Oxisols (Tiessen et al. 1994). *Terra preta* soils have been classified as Cultic Archaeo-anthrosols and *terra mulata* soils as Agric Archaeo-anthrosols (Kämpf et al. 2003).

Bulk density varies from site to site, although it typically increases with depth and has a positive relationship to clay content and a negative relationship with organic carbon (Teixeira and Martins 2003). ADE soils generally show a lighter texture in comparison to deeper horizons and surrounding soils, resulting in higher permeability

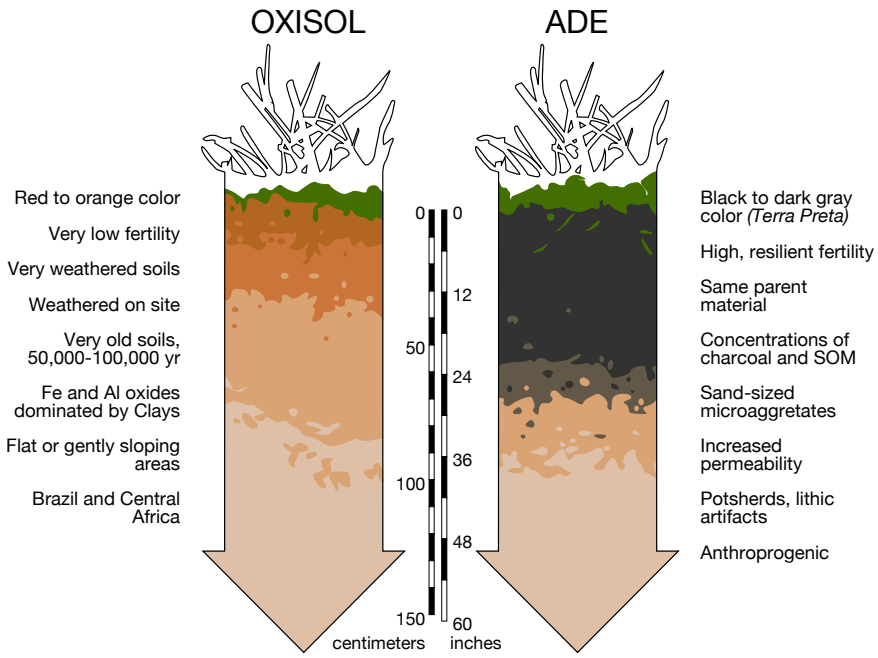

Figure 1.8 Comparison of an Amazonian Dark Earth soil profile with the profile of typical Amazonian Oxisol soils**.** This graphic is based on photographs collected by William Woods. The colors of this graphic are based on the Munsell color system and are the actual colors typical of the soil types.

on ADE sites (Teixeira and Martins 2003). ADE are able to retain water and nutrients despite increased permeability (Lehmann et al. 2003b).

The properties of horizons underlying the ADE soils resemble those of surrounding soils (Glaser 1999; Silva et al. 1970; Sombroek 1966), which indicates that both soils were weathered from the same parent material (Sombroek 1966). Due to the nature of Oxisol soils, nutrient levels are more a factor of soil organic matter (SOM) and nutrient exchange from outside the system than weathering of parent material (Lehmann et al. 2003b). Charcoal, added to ADE, influences nitrogen levels ei-

ther by microbial immobilization due to high carbon to nitrogen ratios or by catalytic effects of the high surface area of the charcoal. Nitrogen availability is better in ADE that in typical Amazonian Oxisols (Lehmann et al. 2003b). Lehmann et al. (2003b) also conclude that ADE contain more available calcium, but not necessarily potassium; that enrichment is often greater at depth; that crop production on ADE for most crops (except those with high potassium requirements) is higher than on the surrounding Oxisols; and that conditions for maximum biological nitrogen fixation were present in ADE. In summary, ADE are high in phosphorus, nitrogen and calcium while being limited in potassium availability (Lehmann et al. 2003b). As a result, ADE exhibit greener vegetation during the dry season (Hartt 1885).

1.6 Soil Organic Matter Stability

The low soil organic matter (SOM) stability in typical Amazonian Oxisols inhibits the agricultural productivity of the region. Amelioration through the application of fertilizers remains ineffective due to the low cation exchange capacity (CEC is essentially the ability of the soils to retain nutrients - Tiessen et al. 1994). SOM, or fertilizers, are quickly decomposed and leached from the soil or, in the case of phosphorus, are quickly immobilized by the high aluminum and iron contest of these soils and rendered unavailable for plant use. ADE soils display much higher levels of SOM stability, a property that seems to be connected to the high levels of charcoal in the soil (Glaser et al. 2003b). ADE soils contain up to 64 times more charcoal than do

typical Amazonian soils (Glaser 1999; Glaser et al. 2001). High levels of charcoal are found in the light fraction of ADE, so a significant portion of the carbon is in particulate form (Glaser et al. 2003b).

Possible vectors through which charcoal supports SOM stability are: 1) chemical resistance due to selective enrichment of stable compounds; 2) chemical binding of organic matter to oxides or clay minerals; and, 3) physical stabilization of easily erodible organic material by entrapment in soil aggregates (Glaser et al. 2003b). In laboratory studies, cumulative leaching of mineral potassium, nitrogen, calcium, and manganese in ADE was only 24, 45, 79 and 7%, respectively of that found in surrounding Oxisols (Lehmann et al. 2003b). Glaser et al. (2003b) found that ADE soils contain more potentially mineralizable SOM, higher sugar levels, and higher amounts of residual SOM in absolute and relative terms than do typical Amazonian Oxisols. Glaser et al. (2003b) conclude by stating that the chemical recalcitrance of charcoal is the main factor responsible for the high SOM stability of ADE.

1.7 Remote Sensing

While many remote sensing studies have been conducted in the Amazon Basin, very few have focused on locating ADE sites. I have found one doctoral dissertation that used satellite imagery to map archaeological sites near the upper Xingu River in Brazil (Russell, 2005). Fortunately, most of Amazonian remote sensing stud-

ies have focused on vegetation and many of their methods can be adapted to locating ADE soils by examining vegetation properties as a surrogate for soil type.

Remote sensing in the Amazon Basin has dealt primary with deforestation and land cover change detection, primarily limited to forest / non-forest classification schemes (Cardille and Foley 2003; Nelson and Holben 1986; Nelson et al. 1987; Skole and Tucker 1993; Wessels et al. 2004). Others have created thematic maps of forest successional stages using extraction and classification of homogeneous objects (ECHO) (Brondizio et al. 1996) and decision-tree classifiers (Lu et al. 2004b). Linear mixture models (LMM), which output a relative abundance of a specified land cover per pixel (see Lu et al. 2004a), have also been used to classify Amazonian forest into seral stages (Asner et al. 2003; Cross et al. 1991). Of particular note, Lu et al. (2003) used LMM to find the percentage cover of shade, bare soil, and green vegetation in Landsat Thematic Mapper images over Rondônia, Brazil. They were able to characterize the forest into four seral stages (initial, intermediate, advanced, and mature forest) with 78.2% accuracy by creating a threshold of the ratio of shade-to-green vegetation. Another LMM approach (Lu et al. 2004a) had difficulty distinguishing between seral stage 1, seral stage 2, pasture and agricultural lands; while seral stage 3 and mature forest were accurately mapped (overall accuracy = 81%). Radar has been used successfully to characterize seral stages (Saatchi et al. 2000), especially along floodplains and seasonally inundated forests (Costa 2004; Rosenquist et al. 2002; Santos et al. 2003).

Several researchers have used reflectance in the middle infrared (MIR) portion of the spectrum to successfully classify Amazonian forest cover into seral stages. Steininger (2000) found a strong relationship between MIR and forest stand structure parameters in Manaus, Brazil. The strongest correlations were between MIR reflectance and stand basal area ($r^2 = 0.72$) and biomass ($r^2 = 0.70$). Salovaara *et al.* (2005) used indicator species (Salovaara et al. 2004) and Landsat ETM+ imagery to accurately characterize three classes of Peruvian Amazon forest near the Brazilian border. The discriminant analysis model made use of a near infra-red (NIR) / MIR ratio and achieved an accuracy of 85% (kappa = 0.62). Vieira et al. (2003) were able to group forest located near Belém, in the Brazilian state of Pará, into four classes of regrowth cover using each pixels' location in feature space when NDVI was plotted against MIR. NDVI alone was not a good indicator of forest age. Lu et al. (2004c) compared 29 vegetation metrics calculated from a single date of Landsat imagery to field-collected forest stand parameters near the Xingu River in Pará State, Brazil. Parameters included aboveground biomass, basal area, average stand diameter and average stand height. The correlation coefficients between these variables and a NIR / MIR ratio were -0.624, -0.526, -0.817, and -0.881, respectively. They conclude that the MIR band and linear transformed indices such as PC1 (the first principal components vector) and KT1 (the brightness component of a tasseled cap transform) and albedo are the most strongly correlated remote sensing variables to forest stand parameters.

Most current efforts to characterize Amazonian forest cover have relied on single dates of imagery [for a review of the Large-scale Biosphere Atmosphere (LBA) in Amazonia project see Roberts et al. 2003]. A notable exception is Xiao et al. (2005). They used multi-year imagery from the VEGETATION sensor onboard SPOT-4 and MODIS data to model gross primary production and determined that the seasonal dynamics evident in EVI and Land Surface Water Index (LSWI) data can be explained, in part, by leaf phenology, leaf age, and leaf water content.

I was able to find a doctoral dissertation that used Landsat imagery to map archaeological sites along the Upper Xingu River in south-central Brazil (Russell 2005). Russell submitted the normalized difference vegetation index (NDVI), the Tasseled Cap Greenness index, the Transformed NDVI, and the simple subtraction vegetation index (SVI) to a principal components analysis (PCA) from which he retained the first two components. He then submitted the soil adjusted vegetation index (SAVI) and the modified SAVI to another PCA and he retained the first component. The bands of the original Landsat scene were submitted to a third PCA and the second and third components were retained. The five retained components were combined with decorrelation-stretched images for bands three and four of the original imagery and then submitted to a supervised maximum likelihood classification. The result was a classified image with 12 classes, including Archaeological Sites Not Under Cultivation and Archaeological Sites Under Cultivation. Russell's overall classification accuracy was 95% with a Kappa of 0.903; however, the producer accuracies for

the two archaeological classes were 78% and 41% and the user accuracies were 41% and 62%.

While Russell's (2005) overall classification was quite accurate, the methods ability to classify archaeological sites was low. Also, Russell studied sites that were likely used on a rotational basis, interspersed with fallow periods. It is hoped that using a time-series approach will increase classification accuracy and allow for classifying ADE sites that have been abandoned for much longer periods of time.

1.8 Conclusion

Amazonian Dark Earths (ADE) were created by the prehistoric inhabitants of the Amazon Basin as they worked to improve the quality of their farmlands. These soils are much more fertile than the surrounding Oxisol soils and they retain their heightened fertility for millennia. Currently, the Brazilian Agricultural Research Agency (EMBRAPA) is investing time and money into learning how ADE soils can be produced today, with the aim of increasing agricultural productivity and reducing dependence on chemical fertilizers (Plate 1.1). This research has the potential to reclaim depleted land and reduce the need for future deforestation. Others are studying whether charcoal, one of the main ingredients in ADE soils, can serve as a long-term carbon storage pool that may slow the effects of possible greenhouse global climate change (Lehmann and Stephen 2009). Studying ADE soils also has the potential of changing the current paradigm regarding historic land use and population dynamics in

the region. This could greatly improve the culture and patrimony of Brazil and other countries that share the Amazon Basin, as well as the topics in general.

Chapter 2

Methods

This chapter has been published with the following reference:

Thayn, J.B., K.P. Price, and W.I. Woods. (2009). Locating Amazonian Dark Earths (ADE) using Satellite Remote Sensing – A Possible Approach. In W.I. Woods, W.G. Teixeira, J. Lehmann, C. Steiner, A. WinklerPrins, and L. Reballato (Eds). *Amazonian Dark Earths: Wim Sombroek's Vision.* Berlin: Springer-Verlag. pp. 279-298.

2.1 Introduction

Amazonian Dark Earths (ADE) are the result of prehistoric humans' occupation of the Amazon Basin and their need to create fertile soils for growing crops (Neves et al. 2003). ADE soils contain highly elevated levels of organic matter, mostly in the form of very slowly decomposing charcoal, which retains water and nutrients, and makes ADE some of the most fertile soils in the world (Kern et al. 2003; Lehmann et al. 2003). When productivity of plants grown on ADE soil was contrasted with typical Amazonian soils, Major et al., (2005) found that maize yields were as much as 63 times greater, weed cover was 45 times greater, and plant species diversity was up to 11 times greater than for adjacent typical Amazonian soils. ADE soils contain up to 70 times more SOM than typical Amazonian soils (Mann 2002). Neves et al., (2003) have shown that nutrient transfers from outside of ADE sites are necessary to explain current nutrient levels in ADE soils, suggesting that the formation of these soils was the result of an intentional effort on the part of

prehistoric Amerindian populations to improve the quality of their farmland. These nutrient sources may have been food wastes, fish bones and other unused fish matter or human excrement. The presence of algae in ADE from ca. 1,150 BP and later suggests that silt from riverbanks was incorporated into the ADE soils in at least one location (Mora et al. 1991).

In addition to opening a window to the past, ADE soils may hold a key to the future. The most readily observed characteristic of ADE soils is their high concentration of charcoal, which gives them their distinctive dark brown-to-black coloration. Glaser et al., (2001) found 64 times more charcoal in ADE soils than in the surrounding soils. To meet the challenges of possible global climate change caused by greenhouse gases, atmospheric carbon concentrations must be reduced. Vegetation actively withdraws carbon from the atmosphere and stores it as organic matter. Biochar is created when organic matter is heated without oxygen and it contains twice the carbon content of ordinary biomass (Lehmann 2007). Biochar is much more resistant to decay and can store carbon for centennial timescales (Lehmann et al. 2006). The addition of biochar to the soil was part of the creation of ADE (Neves et al. 2003). This has lead some to speculate on the viability of a biochar carbon sequestration industry which would reduce atmospheric green house gases (Marris 2006; Sombroek et al. 2002) and improve soil fertility (Lehmann et al. 2003).

ADE range from 2,500 to 500 years old (Neves et al. 2003), so ADE soils offer a unique opportunity to study the long-term carbon storage capacity of biochar

in soils. One factor that restricts this research is a lack of maps detailing the location of ADE sites. While some rudimentary maps exist (Heckenberger et al. 1999), the geographic extent and location of ADE are unknown (Woods 1995). However, Sombroek (2002) estimates that there is a patch of ADE soil for every 2 km^2 along certain Brazilian river corridors, and they extend into Colombia, Venezuela, Peru, Bolivia and the Guianas. Mann (2002) estimates that ADE soils occupy up to 10% of the Amazon Basin – an area equal to the size of France.

Currently known ADE sites were found primarily by local *caboclo* residents who prefer ADE soils for agricultural settlement and subsistence farming (Sombroek et al. 2002). Woods and McCann (1999) report that local residents recognize ADE soils based on their lower vegetation canopy and more closed understory, and unique species compositions including brazil nut (*Bertholletia excelsa*), papaya (*Carica papaya*), cacao (*Theobroma cacoa*), cupuacu (*Theobroma grandiflorum*), and the giant *Ceiba pentandra*. Unfortunately, traditional field methods are unsuited for locating ADE soils for two primary reasons: (1) the extreme difficulties associated with fieldwork in the dense tropical forest; and, (2) the time that would be required to cover the enormous extent of the Amazon Basin. Therefore, most ADE soil sites have not been located. For these reasons, methods for predicting the geographic location and extent of these soils are required. Such information would greatly enhance researchers' ability to find new sites, could contribute to preserving tropical forests in this region, and would assist scientists' efforts to study and replicate ADE soils.

Satellite remote sensing has tremendous potential for locating ADE soils using vegetation seasonal patterns and vigor as a surrogate for soil type.

2.2 Remote Sensing Overview

Before one can appreciate the advantages of using remotely sensed imagery for locating ADE sites, one needs at least a basic understanding of remote sensing system resolutions. The following overview will use the most commonly used remote sensing systems in existence at this time as examples. These systems include the U.S. Landsat Thematic Mapper (TM), the French SPOT, the private sector IKONIS, OrbView-3, and Quickbird, the Terra and Aqua systems that both carry the Moderate Resolution Imaging Spectrometer (MODIS), and the Polar Orbiting Meteorological Satellite that carries the Advanced Very High Resolution Radiometer (AVHRR). Some additional information about these systems will be presented throughout this chapter, but refer to Jensen (2005) for a more complete overview.

2.2.1 Remote Sensing Resolutions

There are four types of resolution that need to be considered when comparing remote sensing systems. These resolutions are: *spatial*, *spectral*, *radiometric*, and *temporal*. The following definitions are adapted from Jensen (2005).

Spatial resolution is a measure of the smallest angular or linear separation between two objects that can be resolved by the remote sensing system. The picture element (pixel) width is often used to describe the spatial resolution. Spatial

resolution of space-borne satellites varies from less than 1 m to 50 km, with most sensors in the 10 to 1100 m range. For example, the Landsat sensor has a nominal spatial resolution of 30 m, meaning that each pixel covers an area of the earth's surface that is 30 m wide and 30 m tall, with an area of 900 m^2. The SPOT sensor has a nominal spatial resolution of 20 m.

Spectral resolution is the number and dimension (size) of specific wavelength intervals (referred to as *bands* or *channels*) in the electromagnetic spectrum to which a remote sensing instrument is sensitive. Higher spectral resolution instruments have either more bands, or narrower bands, or both. Normal spectral resolution of space borne satellites is 3 to 36 bands. Hyperspectral sensors collect 126 to 256 bands.

Radiometric resolution is defined as the sensitivity of a remote sensing sensor to differences in signal strength as it records the radiant flux reflected, emitted, or back-scattered from the terrain. It defines the number of just discriminable signal levels. The human eye can discriminate between 8 and 15 radiant intensity levels, or shades of gray ranging from white to black. The radiometric resolution of space-borne satellites varies from 256 to 1024 intensity levels.

Temporal resolution refers to the frequency with which imagery is collected for the same location. For example, the temporal resolution of the Landsat sensor is 16 days. SPOT has a repeat time of 26 days, but greater temporal resolution can be obtained if off-nadir views of the terrain can be obtained and used. The temporal resolution of the near 1 m resolution systems is 1-5 days, but this is only if one can

use surfaces viewed from an oblique or off-nadir angle. Off-nadir views are obtained on an infrequent basis. The temporal resolution of the National Oceanic and Atmospheric Administration (NOAA) Polar Orbiting Meteorological Satellite that carries the AVHRR sensor (with a spatial resolution of 1 km) is daily worldwide (except for 9 degrees from the north and south poles).

Swath width, which is how wide an area is imaged each time the satellite orbits the planet, is also a critical factor and obviously influences how often the sensor captures data over an area on the earth. The smaller the pixel or the greater the spatial resolution, the narrower the swath width. For example, the swath width of the meter to sub-meter measuring instruments is 8 to 11 km, compared to the 2,600 km width of the coarse resolution 1 km AVHRR data. Therefore, spatial resolution and temporal resolution share an inverse relationship. Anyone beginning a remote sensing based research project must determine which resolution, temporal or spatial, is most important for their application. Recent vegetation monitoring projects have shown that high temporal resolution is often more useful for discriminating vegetation than high spatial resolution because a series of frequent images captures seasonal or phenologic trends (Bradley et al. 2007; Hill and Donald 2003; Jakubauskas et al. 2002; Wardlow et al. 2006; White et al. 2005).

2.2.2 Vegetation Indices

Converting satellite data into meaningful vegetation information involves calculating a vegetation index. Photosynthetically active vegetation, although it

appears green to us, actually reflects more near-infrared light than any other wavelength. Healthy vegetation absorbs red light, which is used to power photosynthesis. There is an inverse relationship between red reflectance and chlorophyll content, and a direct relationship between leaf structure and near-infrared reflectance. Therefore, as vegetation density increases, more near-infrared light and less red-light are reflected. This inverse relationship is the foundation for most vegetation indices, which estimate the amount of photosynthetically active vegetation present in each pixel of satellite imagery. The most common of these indices is the normalized difference vegetation index (NDVI)(Rouse et al. 1973):

$$NDVI = \frac{NIR - R}{NIR + R} \tag{1}$$

Where *NIR* is near-infrared reflectance and *R* is red light reflectance. NDVI has been used successfully around the world (Dennison et al. 2005; Hill and Donald 2003; Oindo 2002; Shilong et al. 2004; Wang et al. 2004). The strong correlation between the NDVI and green photosynthetically active vegetation has caused some to refer to the NDVI as a plant "greenness" index. However, NDVI tends to saturate in locations with very dense vegetation, such as in the Amazon Basin. A modification of the NDVI, the enhanced vegetation index (EVI) has been developed specifically for the MODIS sensor:

$$EVI = G\frac{NIR - R}{NIR + C_1 RED - C_2 B + L}(1 + L) \tag{2}$$

Where G is green reflectance and B is blue reflectance. L is a soil adjustment factor and C_1 and C_2 are coefficients, which describe the use of the blue band in correcting red reflectance for atmospheric scattering. The coefficients L, C_1 and C_2 have been determined empirically to be 6.0, 7.5 and 1.0, respectively. EVI exhibits less saturation in tropical regions than many vegetation indices (Didian 2002), is related to forest stand biomass (carbon storage, Roberts et al. 2003), to tropical forest leaf litterfall (Saleska et al. 2003; Xiao et al. 2005), to leaf canopy processes (Xiao et al. 2005), and is more sensitive to seasonal dynamics than other vegetation indices (Ferreira et al. 2003). For research in the Amazon Basin, the EVI is suggested.

2.2.3 Maximum Value Composite Images

While satellite sensors frequently capture images of the earth's surface, cloud cover or other aerosol contaminants will obstruct many of these images. One major advantage of using satellite systems with high temporal resolution is the ability to construct maximum value composite (MVC) vegetation index images. Pixels with cloud contamination have depressed NDVI or EVI values and are not an accurate estimate of vegetation biomass. The MVC procedure groups a series of sequential satellite images and selects the maximum value of each pixel from the series (Holben 1986). The underlying theory is that, since cloud contamination lowers the NDVI or EVI value, a maximum value composite represents the most cloud-free pixel from the compositing period. The Advanced Very High Resolution Radiometer (AVHRR), the Moderate Resolution Imaging Spectroradiometer (MODIS), the Vegetation sensor,

and the ENVISAT sensor have sufficient temporal resolution to routinely compute MVC images. The imagery collected by the AVHRR is composited from 14-day periods and MODIS imagery is composited from 16-day periods. The ability to create MVC images is essential to any satellite-based remote sensing project undertaken in the Amazon Basin, where cloud cover frequently obscures surface vegetation.

While maximum value compositing reduces the effects of cloud cover, it also introduces temporal error. The MVC process selects the maximum value of the composite period and creates a single image, which is typically assigned the first date of the composite period. When using satellite vegetation indices to model vegetation seasonal patterns, knowing the Julian date of each index value is critical. Researchers attempting to calculate seasonal or phenologic variables from a time-series of sequential images have been forced to make assumptions regarding the date of each value. Many researchers, possibly for the sake of simplicity, have used the assigned first date of the period. This is the same as assuming that the maximum amount of photosynthetic activity during each composite period happens at the beginning of the period. This assumption is logical during the fall or senescence periods where vegetation vigor is steadily declining. However, during the spring or greening-up period, the more logical assumption is that the maximum value of the period occurs at the end of the period since photosynthetic activity is steadily increasing (see Wardlow et al. 2006 for a further discussion). However, recent work at the Kansas Applied Remote Sensing (KARS) Program at the University of Kansas has been unable to find

a strong relationship between the actual Julian Date and its location within the composite period, indicating that methods based on these assumptions contain inherent error (Thayn and Price, 2008).

In order to determine the extent of the error introduced by using the end-of-the-period assumption, over 2000 random points were selected within Douglas County, Kansas. The onset of green-up metric (Reed et al. 1994) was calculated using the Zhang method (Wardlow et al. 2006; Zhang et al. 2003) and MODIS NDVI imagery from 2001. The onset of green-up is the date at which vegetation begins to bloom at the beginning of spring. The Zhang method fits a monotonic function to an annual time-series of vegetation index values. The Julian date corresponding to the maximal point of the rate of curvature of the monotonic function is selected as the date of vegetation green-up (see below for more further explanation of the Zhang method). The onset metric was calculated twice, once using the last date of the composite period and once using the actual Julian date of each pixel. While the correlation between the two sets of onset dates was high (r^2 = 0.80), the root mean square error between the two was large, essentially equal to the interval of the composite period (rmse = 15.91) (Fig. 1). A

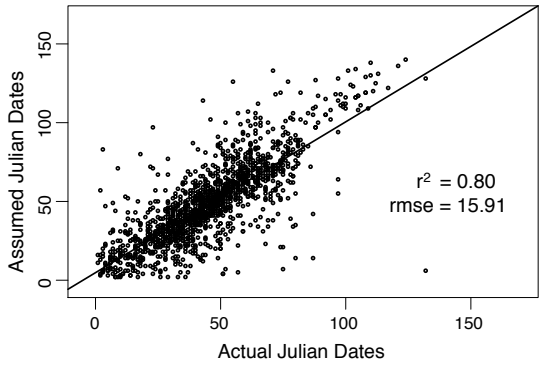

Figure 2.1: Temporal error introduced by the Maximum Value Composite (MVC) process.

potential error of half a month is a critical flaw in any project attempting to quantify seasonal patterns.

Beginning with version 5 of the MODIS data, the Julian date of each pixel selected in the MVC procedure is reported, eliminating the temporal error created by maximum value compositing. MODIS imagery is the only satellite data currently available with the Julian date information. At the time of this writing, the EROS Data Center offers 2007 satellite imagery as version 5 data and has started re-processing previous years. The anticipated completion date of this back-processing is mid-2008.

2.2.4 Remote Sensing System Requirements

As stated in the previous sections, the major purpose for using remotely sensed imagery is to locate Amazonian Dark Earth (ADE) sites that are currently hidden beneath the tropical forest canopy of the Amazon Basin. For this project, we determined that there are a least six requirements for a satellite system that must be met. These requirements are:

1. Conterminous spatial coverage of the Amazon Basin
2. High temporal resolution in order to create maximum value composite images to minimize interference from cloud cover and to capture seasonal variation in vegetation
3. Adequate spatial resolution to resolve patches of ADE soil
4. Sufficient radiometric and spectral resolution to calculate NDVI or, preferably, EVI values

5. The Julian date of each pixel selected during the maximum value composite process needs to be reported
6. Low cost of image acquisition

The only remote sensing system to meet all of these criteria is the MODIS sensor flown on NASA's *Terra* and *Aqua* satellite platforms. MODIS data are preprocessed as normalized difference vegetation index (NDVI) values and enhanced vegetation index (EVI) values. For reasons stated above, we suggest using the EVI. While most remote sensing systems collect imagery at a nadir viewing angle over an area once every 16 to 26 days, the MODIS sensor collects images over an area at least once daily, and because there is normally a morning and afternoon overpass by the Terra and Aqua orbiting platforms, MODIS imagery are often captured over an area twice daily. EROS Data Center computes maximum value composite (MVC) Enhanced Vegetation Index (EVI) images from 16-day periods resulting in an annual time-series of 23 images. The maximum EVI composites are created using the MODIS 250, 500, and 1 km resolution images. The images from each satellite are processed separately, creating two annual time-series of EVI data. In previous Amazonian work, we have merged the composites from the Terra and Aqua systems to create dual-system very near cloud-free EVI composites (Brown et al. 2007). These dual-system composites are more cloud-free than the original, single-system composites. These datasets have been produced for 2000 to the present. It is

anticipated that these datasets will continue to be produced until the MODIS system becomes inoperable.

The spatial resolution of the imagery is 250-meters (~15 acres per pixel) which is adequate for detecting ADE patches which range in size from 5 to 30 hectares (Sombroek et al. 2002). MODIS scenes measure 1,200 km^2 and are distributed free of charge and are preprocessed to correct for atmospheric effects and to screen for clouds. Morton et al. (2006) further eliminated cloud contamination using a weighted cubic spline process. An example of a dual system maximum value composite, before and after cubic spline smoothing, is presented in Fig. 2. Another option is the 4253H-twice filter (Velleman 1980), which was found to be the most accurate of six smoothing filters tested by Klassen and McDermid (2007).

2.3 Past Remote Sensing Research in Amazonia

The use of satellite remotely sensed data for mapping tropical forests of the Amazon began in earnest with efforts to detect and monitor deforestation in the 1980s (Malingreau and Tucker 1988; Nelson et al. 1987; Skole and Tucker 1993). These projects focus primarily on differentiating between forest and cleared pasturelands rather than characterizing forest cover. More recently, the Large-Scale Biosphere-Atmosphere Experiment in Amazonia (LBA) has examined the forest with greater detail by categorizing it into successional stages (Roberts et al. 2003). Most of these projects use a single date, or a few dates, of high spatial resolution imagery, such as

Landsat TM, SPOT-4 and Ikonos imagery, and analysis methods such as linear spectral mixture modeling to estimate biomass. See Brown et al. (2007) for an excellent review of past remote sensing based studies of the Amazon Forest.

While most remote sensing projects in the Amazon Basin do not attempt to classify or characterize forest cover, there are a few exceptions. Lu et al. (2003) used Landsat Thematic Mapper (TM) imagery and linear mixture modeling to classify Amazonian forest from the Brazilian state of Rondônia. A linear mixture model calculates the percent cover, per pixel, of a pre-determined land cover type. Due to the mathematics involved, the number of pre-determined land cover types is limited. In this study, three pre-determined land cover types were used: shade, soil, and green vegetation. Lu and his colleagues were able distinguish Initial, Intermediate, and Advanced successional stages of forest growth with 78.2% accuracy. They conclude that the shade and green vegetation fractions are sensitive to change in vegetation stand structure and are therefore able to capture biophysical structure information. Although there is colloquial evidence that stand structure and forest biophysical parameters are

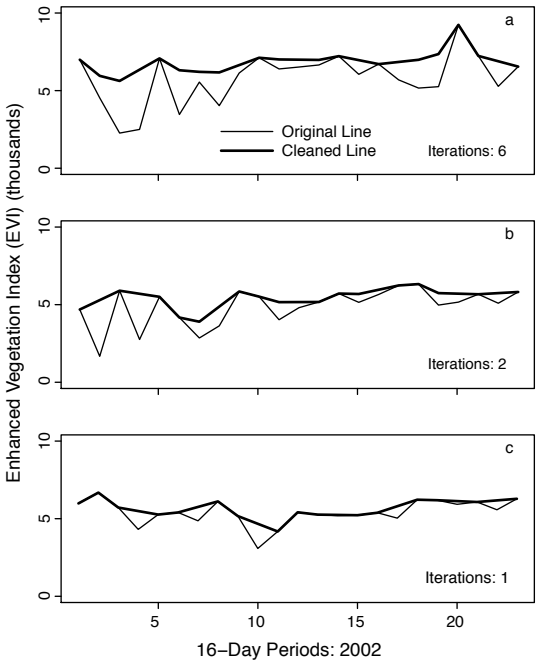

Figure 2.2: Three examples of smoothed annual EVI signatures from Manaus, Brazil.

possible ADE soil identifiers (Woods and McCann 1999), this method is limited in that it characterizes forest cover based on a single satellite image, or a single moment in the seasonal pattern of the vegetation. We hypothesize that locating ADE soils will require the analysis of a complete seasonal pattern.

Steininger (2000) used Landsat TM imagery to estimate above-ground biomass in the Amazon Basin. He discovered a strong correlation between mid-infrared reflectance and stand age, height, volume and biomass ($r > 0.80$, $p < 0.01$), although this relationship saturated at around 15 kg m^2 of biomass or at about 15 years of stand regrowth following deforestation. Vieira et al. (2003) was able to discern 4 successional stages in the forests of Pará, Brazil. They determined that the normalized difference vegetation index (NDVI) was insufficient for classifying forest cover. They, like Steininger (2000), found a strong relationship between mid-infrared reflectance and stand biophysical variables. The mid-infrared portion of the electromagnetic spectrum has been associated with water content in vegetation. Salovaara et al. (2005) used a ratio of the near-infrared band and the mid-infrared band from Landsat imagery to map inundated Amazonian forest with 85% accuracy.

2.4 Vegetation Vigor

The ability to distinguish forest cover growing on ADE soils from forest growing on typical Amazonian soils is more complicated than characterizing forest cover into successional or seral stages. The differences between forest parameters that

are indicative of soil type are much more subtle, and therefore much more difficult to detect. We hypothesize that the most reliable differences in vegetation growing on ADE soils and that growing on typical Amazonian soils will be plant vigor. As early as 1885 (Hartt) it was reported that vegetation growing on ADE soils is more photosynthetically active during the dry season than vegetation growing on the surrounding Oxisols. Hartt attributed this difference to increased soil moisture associated with the ADE soils. Glazer et al., (2003) found ADE soils to contain 2.75 times more silt and 0.25 times more coarse sand than was found in the surrounding soils, making them more permeable and able to retain more soil moisture at greater depths (Lehmann et al. 2003). Tropical forest trees survive the six-month dry season by tapping into moisture reservoirs in the soil and as the dry season progresses soil moisture reserves at increased depths become more important to survival, especially in severely dry years (Jipp et al. 1998; Nepstad et al. 1994). This means trees on ADE soils have a greater chance of survival during severe drought conditions and, to the extent that available soil moisture influences plant phenological processes (greening patterns), trees on ADE soils will exhibit different growth rates and timing of photosynthesis activities throughout the year. In a year with typical precipitation, Amazonian forests are not greatly affected by the dry season. In fact, photosynthesis and leaf production are limited during the wet season because of cloud cover and peak during the dry season when leaves have access to more light (Huete et al. 2006; Saleska et al. 2003). A partial rain throughfall exclusion experiment indicates that

water stress to vegetation is minimal during a drought year. Stress occurs the year following drought, when soil moisture has been expended but not replenished (Nepstad et al. 2002). Record drought occurred in Brazil in 2005, so satellite imagery collected in 2006 offers a promising opportunity to locate ADE sites.

Current annual time-series research in the Amazon Basin indicates that remote sensing techniques would be sensitive to the differences between vegetation grown on ADE soils and that grown on typical Amazonian soils (Heckenberger et al. 2003; Huete et al. 2006; Nepstad et al. 1994; Nepstad et al. 2002; Saleska et al. 2003). In particular, Morton et al*.,* (2006) used minimum, maximum, mean, median and harmonic variables (amplitude and phase of a sin/cosine curve fitted to the annual EVI pattern) calculated from annual EVI and NDVI time-series' to classify landcover in Mato Grosso, Brazil as either cropland, cattle pastureland or regrowth forest. They were able to determine the conversion rates of forest to cropland from 2001 to 2004. This methodology is similar to that which we propose in this chapter. Harmonic analysis was used by Brown et al. (2007) to characterize the intensification of agricultural lands in Vilhena, Brazil. First- and second-order harmonic components were calculated from the annual time-series. A first-order harmonic is sin/cosine curve with a frequency of one that has been fitted to the series. The second-order harmonic is the best-fit sin/cosine curve that has a frequency of two (Fig. 3). If the amplitude of the second harmonic was greater than or equal to the amplitude of the

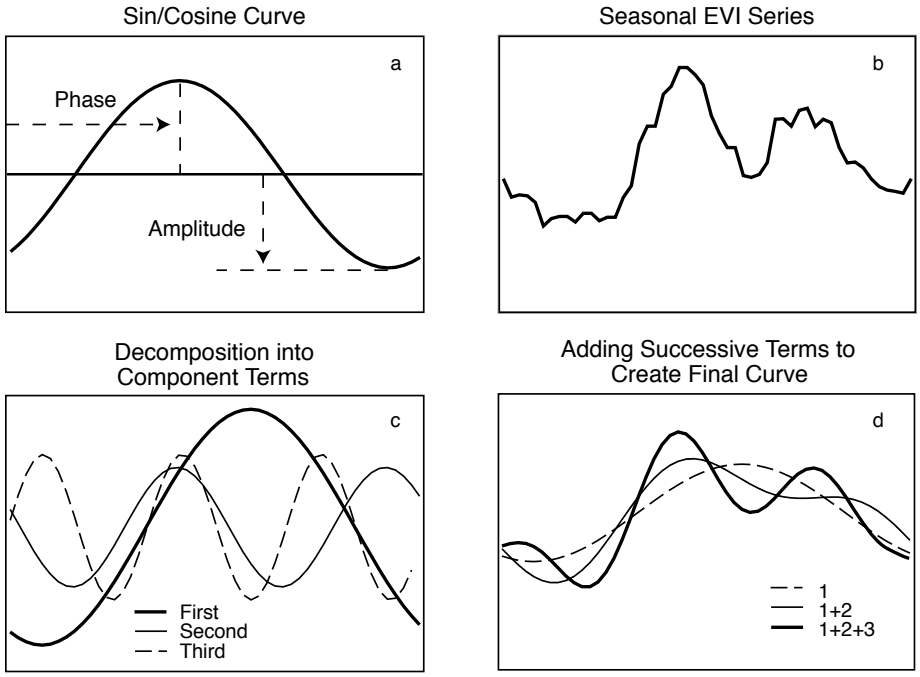

Figure 2.3: Examples of Harmonic Wave Analysis properties: a) each harmonic curve is defined by a phase and an amplitude, b) an annual EVI signal of a double-cropped agricultural site, c) the annual signal decomposed into its first three harmonic waves, and d) the sum of the harmonic waves approximates the original EVI signal.

first harmonic, then the pixel was assigned to the double crop intensification class. The accuracy of this classification was approximately 80%.

One (or even several) satellite image is unlikely to capture the subtle distinction in vegetation vigor that occurs between ADE and non-ADE forests during water stress conditions. An annual time-series of satellite images is required to visualize and quantify the differences in plant vigor that are symptomatic of ADE soils. Our preliminary work over known ADE sites has shown that the differences in phenological patterns are detectable using time-series analysis approaches. Therefore, the solution to identifying ADE sites appears to lie in the use of coarser spatial

resolution imagery (250-meter pixel width), which increases the frequency at which images over an area can be acquired. Increased temporal coverage by finer spatial resolution satellite imaging systems, like Landsat, would be possible if multiple systems were placed in a proper earth-orbiting configuration, but such configurations do not exist at this time. Increased temporal resolution image datasets not only help resolve the differences in plant seasonal patterns, but it also greatly diminishes the problems of cloud cover contamination in the imagery; a problem that has plagued past studies conducted in the Amazon Basin.

2.5 Proposed Methods

A method for quantifying or characterizing the seasonal pattern captured in a time-series of remotely sensed images is required. Two likely candidate methods, Harmonic Wave Analysis and the Zhang method of determining phenologic variables, are discussed below.

2.5.1 Harmonic Wave (Fourier) Analysis

Harmonic wave analysis (HWA) permits a complex curve, such as an annual time-series vegetation index signal, to be expressed as the sum of a series of cosine waves. Each of these waves is defined by a unique phase and amplitude (Fig. 3a). The term of each wave designates the number of wavelengths completed over the chronological range of the data. Successive harmonic terms are added to produce a more complex curve, approximating the original signal (Fig. 3d). The lower order

waves (1, 2, etc.) demonstrate trends in the data, while the higher order waves (n, n-1, etc.) contain mostly noise (Jakubauskas et al. 2001). The sum of all of the component curves reproduces the original signal (Jakubauskas et al. 2001; Olsson and Eklundh 1994). A literature review discovers few Amazonian applications of harmonic analysis and, of those, most are precipitation pattern studies (de Angelis et al. 2004a, b).

The equations for calculating the amplitude and phase of a vegetation index signal are:

$$amplitude = \sqrt{C_f(x) + S_f(x)} \tag{3}$$

$$phase = \arctan\left(\frac{C_f(x)}{S_f(x)} \right) \tag{4}$$

If $C_f(x)$ is less then zero than π is added to the phase. The equations for $C_f(x)$ and $S_f(x)$ are:

$$C_f(x) = \sum_{i=1}^{n} \left(i \times \cos\left(\frac{2\pi x f}{n} \right) \right) \times \frac{2}{n} \tag{5}$$

$$S_f(x) = \sum_{i=1}^{n} \left(i \times \sin\left(\frac{2\pi x f}{n} \right) \right) \times \frac{2}{n} \tag{6}$$

where n is the number of points in the series, x is the temporal unit of each point, j is the VI value for each x, and f is the term of the harmonic being calculated.

When calculated from an annual time-series EVI signal, harmonic analysis summarizes patterns in vegetation dynamics in two terms, the amplitude and the

phase. The amplitude of the first harmonic indicates the variability of productivity over the year as expressed in a single annual pulse of net primary production. The phase of the first harmonic summarizes the timing of vegetation green-up and senescence (i.e., the start and ending of the productive growing season) relative to seasonal climatic events. The second harmonic indicates the strength (amplitude) and timing (phase) of any biannual signal, such as secondary vegetation types like subcanopy grasses or secondary tree species. The 0^{th}-order harmonic, or the mean value of the series, indicates overall productivity. The amplitude and phase of the lower-order harmonics have been used successfully in land cover/land use classification and works especially well in differentiating vegetation functional groups (Brown et al. 2007; Jakubauskas et al. 2001; Moody and Johnson 2001). When calculated for multiyear data sets, harmonic signals can be used to detect interannual patterns such as El Niño/Southern Oscillation events (Olsson and Eklundh 1994).

Harmonic analysis is particularly suited for application in neotropical forests like those of Amazonia. Harmonic waves extract primary vegetation phenology trends and reduce the effects of noise in the data (Jakubauskas et al. 2001). This is especially useful in tropical forest zones that experience frequent cloud cover and aerosol contamination from deforestation fires. Harmonic analysis has been used to reconstruct nearly noise-free data sets by computing the component waves and summing only the lower-order waves (Jakubauskas et al. 2002). This method has

been used to reconstruct cloud-free time-series vegetation index data sets (Jun and Zhongbo 2004; Jun et al. 2004).

When calculated from an annual time-series vegetation signal, harmonic analysis summarizes patterns in vegetation dynamics in two terms, the amplitude and the phase. The amplitude of the first harmonic indicates the variability of productivity over the year as expressed in a single pulse of net primary production. The phase of the first harmonic summarizes the timing of vegetation green-up and senescence (i.e., the start and end of the growing season). The second harmonic indicates the strength (amplitude) and timing (phase) of any biannual signal. The additive term of the harmonic series, or the mean value of the data signal, indicates overall productivity. The amplitude and phase of the lower-order harmonics have been used successfully in land cover/land use classification and works especially well in differentiating vegetation functional groups (Jakubauskas et al. 2001; Moody and Johnson 2001). Examples of three vegetation signals from the study site, superimposed by their first harmonic wave, are displayed in Fig. 4.

We hypothesize that Harmonic Wave Analysis will capture the seasonal differences of vegetation growing on ADE soils verses non-ADE soils. The increased vegetation greenness associated with ADE soils will be indicated by lower amplitude values (caused by decreased seasonal variation as vegetation retains greenness during the dry season) and by larger phase angles (caused by a longer growing season). Vegetation growing on ADE soils will also display a larger additive term associated

with increased overall annual net primary production. An example of a first harmonic wave, calculated for ADE and non-ADE soils, is presented in Fig. 5. Notice that although the means of the two signals are very similar, the amplitude and phase values are significantly different. A partial rain throughfall exclusion experiment conducted in the Tapajós National Forest in Brazil indicated that severe water stress occurs the year following drought when soil moisture has been expended, but not replenished (Nepstad et al. 2002). Increased water stress will exaggerate the seasonal variation on non-ADE soils (causing amplitude values to increase and phase angles to be lower), making it easier to recognize ADE soils during these end-of-drought periods.

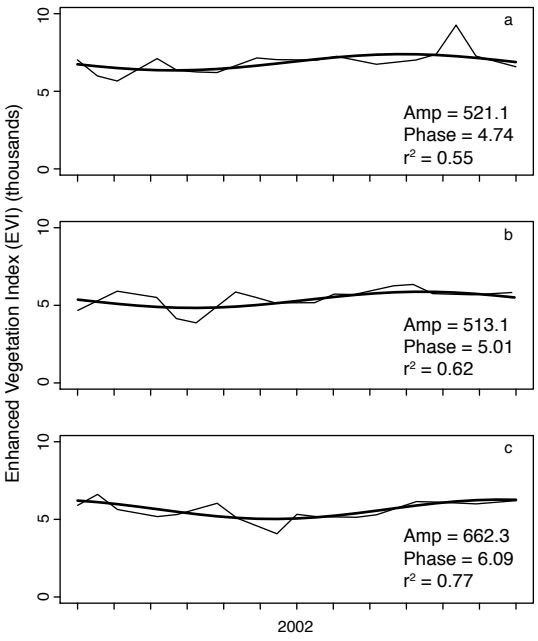

Figure 2.4: Three examples of annual EVI signatures from Manaus, Brazil superimposed by their first harmonic curve. The r^2 is that of the curve to the original signal.

2.5.2 Vegetation Phenology Metrics

Phenology refers to the timing of changes in vegetation as a response to seasonal changes such as temperature and precipitation. The three key phenologic variables estimated using satellite remote sensing are onset of greenness (OG, the start of the growing season), the end of greenness (EG, the end of the growing season), and the length of the growing season (LG). When using satellite imagery to derive phenology characteristics, the object is

not species or population phenology, but that of the general, pixel-wide plant community (Reed et al. 2003).

There are several methods for deriving phenology estimates using satellite imagery (Reed et al. 2003), but most are able to select phenologic variables from only the dates represented by the time series of imagery. Zhang et al., (2003) provide a method that can estimate phenologic variables for dates that fall between image dates. The methodology uses a piecewise logistic function that fits an s-curve to the temporal curve of the satellite imagery. The rate of change of the curvature of the logistic s-curve is calculated and the first peak or maximal value corresponds to the onset of greenness (Fig. 6). This is the point on the s-curve where the line first begins to climb – this estimates the date where vegetation first begins to photosynthesize beyond the background value.

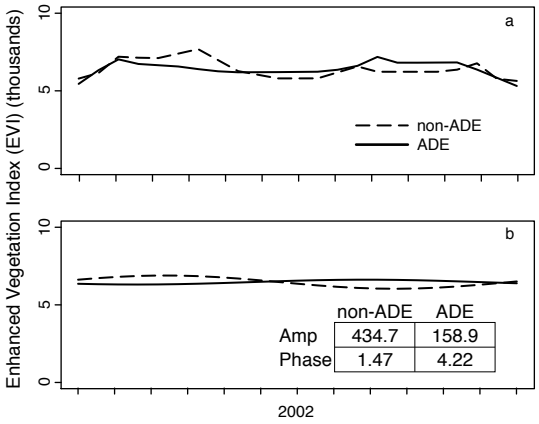

Figure 2.5: An Amazonian Dark Earth (ADE) site compared to a non-ADE site near Santarém, Brazil; a) shows the smoothed EVI signals and b) shows the first harmonic curve.

The s-curve is derived using the equation:

$$y(t) = \frac{c}{1 + e^{a+bt}} + d \qquad (7)$$

where t is time in days, $y(t)$ is the VI value at time t, a and b are fitting parameters, $c+d$ is the maximum VI values, and d is the initial background VI value. Zhang et al. (2003) optimized a and b and treated c and d and constants. However, Wardlow et al. (2006) were able to generate a better fit, and a more intuitive result, by optimizing c and d as well. The optimization was seeded using the definitions above.

Once a, b, c, and d have been found, the s-curve can be reconstructed to give daily values, effectively extrapolating between image capture dates. This would create a daily NDVI or EVI value as modeled by the logistic function. The mathematics of this process are robust enough to allow for irregularly spaced input values, so the actual Julian date of each pixel from within the composite periods could be used. As discussed earlier, this greatly increases the accuracy of the results.

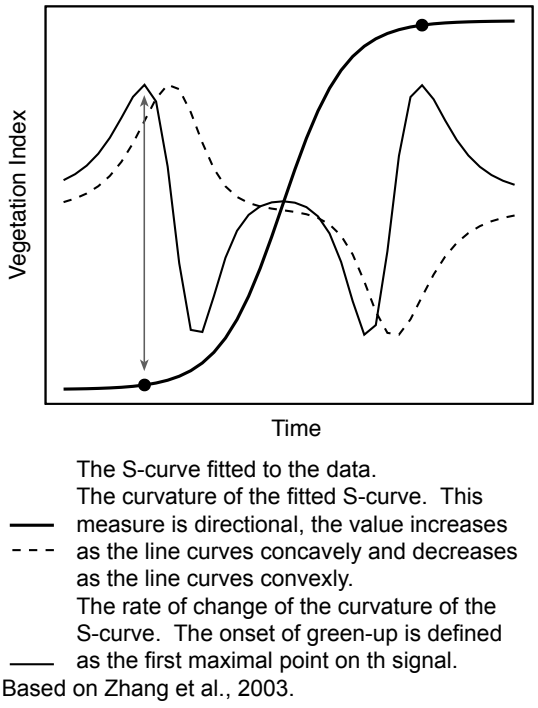

Figure 2.6: Schematic of the Zhang method of onset of greenness identification.

The rate of change in the curvature of the fitted logistic s-curve is used to estimate phenological transition dates. The equation for the curvature of the s-curve follows:

$$K = \frac{d\alpha}{ds} = -\frac{b^2 cz(1-z)(1+z)^3}{\left[(1+z)^4 + (bcz)^2\right]^{\frac{3}{2}}} \tag{8}$$

where $z = e^{a+bt}$, $\propto$ is the angle (in radians) of the unit tangent vector at time t along a differentiable curve, and s is the unit length of the curve. The rate of change of the curvature is:

$$K' = b^3 cz\left\{\frac{3z(1-z)(1+z)^3\left[2(1+3)^3 + b^2c^2z\right]}{\left[(1+z)^4 + (bcz)^2\right]^{\frac{5}{2}}} - \frac{(1+z)^2\left(1+2z-5z^2\right)}{\left[(1+z)^4 + (bcz)^2\right]^{\frac{3}{2}}}\right\} \tag{9}$$

The end of greenness is found by repeating the process at the senescence portion of the EVI time series. The length of the growing season is found by subtracting the onset of greenness from the end of greenness. During water stress years in the Amazon Basin, vegetation growing on ADE soils will have a longer growing season than vegetation growing on the surrounding oxisols due to their greater permeability and soil moisture capacity.

Another potential means of applying this method to locating ADE sites is to calculate the onset of senescence. This is the date at which vegetation begins to loose vigor and "greenness" due to annual water stress near the end of the dry season. As mentioned earlier, the onset of senescence will be more apparent during drought years or the year following a drought year. Under these conditions, the onset of senescence

will be significantly delayed for vegetation growing on ADE soils compared to vegetation growing on non-ADE soils.

2.6 Conclusion

Amazonian Dark Earths (ADE) are the incredibly fertile soils created by prehistoric inhabitants of the Amazon Basin to increase food production for growing populations (Neves et al. 2003; Woods 2003). Finding and studying these soils will help understand the size and cultural complexity of pre-Columbian inhabitants and will enrich the cultural heritage of those nations that contain part of the Amazon Basin. In addition to offering a window to the past, ADE soils have the potential of effecting our future. Reproducing ADE soils would sequester atmospheric carbon in a stable, long-term form that would reduce the effects of possible climate change (Lehmann 2007; Marris 2006), while also increasing agricultural production (Sombroek 1966; Sombroek et al. 2002). One of the greatest impediments to studying ADE soils is that many ADE sites remain hidden beneath the tropical forest. The extreme difficulties of performing ground surveys in so dense and so large a region make traditional methods ineffective at locating ADE sites. Satellite remote sensing is potentially the most effective and economical way of locating ADE sites in the Amazon Basin.

While the methods proposed in this chapter have yet to be fully tested, early trials suggest that they will be effective at locating Amazonian Dark Earths by

examining vegetation vigor as a surrogate for soil type. Based on literature review and preliminary studies conducted thus far, several conclusions can be drawn regarding locating currently unknown ADE sites:

1. Satellite remotely sensed imagery is the most efficient tool for locating Amazonian Dark Earths (ADE) in the Amazon Basin.
2. The most reliable distinction between vegetation growing on ADE soils and vegetation growing on non-ADE soils will be the higher vigor and robustness of vegetation growing on ADE soils during times of water stress.
3. An annual time-series of imagery is needed to detect the subtle increase in vegetation vigor of vegetation growing on ADE soils. Locating ADE soils in the Amazon Basin using satellite imagery will be accomplished by examining vegetation seasonal pattern as a surrogate for soil type.
4. The Moderate Resolution Imaging Spectroradiometer (MODIS) instrument aboard NASA's Terra and Aqua satellites is the most appropriate satellite sensor for locating ADE soils. MODIS data are collected twice daily for every part of the earth's surface, allowing for the creation of nearly cloud-free maximum value composite (MVC) images. An annual time-series of MODIS MVC images consists of 23 images spaced throughout the year.
5. Candidate methods for analyzing time-series of satellite images include: harmonic wave analysis and the Zhang method (Zhang et al. 2003) for determining the onset of green-up.

Future research will examine these conclusions in greater detail and will apply these methods to locating Amazonian Dark Earths.

Chapter 3

Application of Methodology

3.1 Introduction

Scattered throughout the typically nutrient-poor Oxisol soils of the Amazon Basin are relatively small patches of dark, very fertile soils called Amazonian Dark Earths (ADE - Woods and McCann 1999). ADE contain highly elevated levels of organic matter, mostly very slowly decomposing charcoal, which causes the soil's dark coloration (Kern et al. 2003). The charcoal content of ADE soils is typically four times higher than that of neighboring soils but can be as high as 70 times higher (Glaser et al. 2001). The inert charcoal makes nutrients in the soil more recalcitrant (Glaser et al. 2003; Lehmann et al. 2003b; Steiner et al. 2007) and accordingly, ADE soils are some of the most fertile in the world (Kern et al. 2003; Lehmann et al. 2003a; Tiessen et al. 1994). When productivity of plants grown on ADE soil was contrasted with that of typical Amazonian soils, Major et al. (2005) found that maize yields were as much as 63 times greater, weed cover was 45 times greater, and plant species diversity was up to 11 times greater than for adjacent typical Amazonian soils. In a controlled experiment, Steiner et al. (2007) found that crop production on sites where fertilizer and charcoal had been applied was double that of sites where fertilizer alone had been used.

While charcoal helps retain nutrients that would otherwise be weathered from the soil, nutrient transfers from outside of ADE sites are necessary to explain current

nutrient levels in ADE (Neves et al. 2003; Woods and McCann 1999). This suggests that the formation of ADE soils ultimately became an intentional effort of prehistoric Amerindian populations to improve the quality of their farmland (Neves et al. 2003; Woods and McCann 1999). These nutrient sources may have been plant and animal food wastes, fish bones, other unused fish matter, human urine excrement, and plant materials used for fuel and construction. The presence of algae in ADE from ca. 1,150 BP and later suggests that silt from riverbanks was incorporated into an ADE in Colombia in at least one location (Mora et al. 1991).

Locating and studying ADE sites is important not only from an archaeological and a cultural heritage perspective, but also for its potential as a means for long-term carbon sequestration. To meet the challenges of possible global climate change caused by greenhouse gases, atmospheric carbon concentrations must be reduced. Vegetation actively withdraws carbon from the atmosphere and stores it as organic matter. Charcoal, or biochar, is created when organic matter is heated without oxygen and it contains twice the carbon content of ordinary biomass (Lehmann 2007). The addition of biochar to the soil was part of the creation of ADE (Neves et al. 2003). Studies of known ADE sites, which range in age from 500 to 2,500 years old (Neves et al. 2003), reveal that biochar is resistant to decay and can store carbon for centennial timescales (Lehmann et al. 2006). This has lead some to speculate on the viability of a biochar carbon sequestration industry which would reduce atmospheric

carbon (Lehmann et al. 2006; Marris 2006; Sombroek et al. 2002) and improve soil fertility (Glaser and Woods 2004; Lehmann et al. 2003a; Woods et al. 2009).

While some maps of ADE exist for relatively small subregions (Heckenberger et al. 1999; Kern et al. 2003), the geographic extent and location of ADE are unknown in the major portion of the Amazon Basin (Woods 1995). Nonetheless, Sombroek et al. (2002) estimate that there is a patch of ADE for every 2 km^2 along certain Brazilian river corridors, and that they extend into Colombia, Venezuela, Peru, Bolivia and the Guianas. ADE patches range in size from 0.5 to 300 hectares (Sombroek et al. 2002; Woods and McCann 1999), although 80% of known ADE sites are less than 2 hectares (Kern et al. 2003).

Most known ADE sites were found by local *caboclo* residents who prefer ADE soils for agricultural settlement (Sombroek et al. 2002). ADE are recognized based on their lower vegetation canopy, more closed understory, and unique species compositions, including Brazil Nut *(Bertholletia excelsa)*, cacao *(Theobroma cacoa)*, cupuaçu *(Theobroma grandiflorum)*, and the giant *Ceiba pentandra* (Woods and McCann 1999). ADE soils also contain copious amounts of pottery shards (Neves et al. 2003; Sombroek 1966). Unfortunately, traditional field methods are unsuited for locating ADE for two primary reasons: (1) the extreme difficulties associated with fieldwork in the dense, inaccessible tropical forest; and, (2) the time and expense that would be required to cover the enormous extent of the Amazon Basin. For these reasons, remote sensing-based models that predict the location of ADE sites are

required. Such models would greatly enhance researchers' ability to find new sites, could contribute to preserving tropical forests, and would assist scientists' efforts to study and replicate ADE for carbon sequestration.

The main difficulty with developing such a model is that most known ADE sites have been converted to agriculture with different crop types. Identifying ADE in those conditions is confounded by the varying spectral properties of different crops. Those few known sites that have not been converted to agriculture are located under dense tropical forest canopies which completely occlude the underlying soil so that direct imaging of bare soil is impossible. The goal of the present study is to develop a remote sensing method for locating ADE sites using remotely sensed measures of forest vegetation as a surrogate for soil type.

Very little research has been done exploring the possibility of using remotely sensed data to locate ADE. Most comparable research has focused on studying forest succession and mapping seral stages (Kimes et al. 1998; Lu et al. 2003; Roberts et al. 2003; Salovaara et al. 2005; Steininger 2000; Vieira et al. 2003). Thayn et al. (2008) and Meddens (2006) both discuss possible methods for identifying ADE using remotely sensed data and present small, inconclusive pilot studies.

Russell (2005) predicted the location of archaeological sites on the upper Xingu River in southern Brazil using Landsat TM data with an overall accuracy of 95% and a Kappa of 0.90. Russell (2005) submitted the normalized difference vegetation index (NDVI), the Tasseled Cap Greenness index, the Transformed NDVI,

and the simple subtraction vegetation index (SVI) to a principal components analysis (PCA) from which he retained the first two components. He then submitted the soil adjusted vegetation index (SAVI) and the modified SAVI to another PCA and he retained the first component. The bands of the original Landsat scene were submitted to a third PCA and the second and third components were retained. The five retained components were combined with decorrelation-stretched images for bands three and four of the original imagery and then submitted to a supervised maximum likelihood classification. The model was based on approximately 300 training sites and the accuracy assessment was performed using approximately 100 validation points collected by other researchers and local inhabitants using Global Positioning System (GPS) units (Russell 2009). All surveyed ground sites fell within an approximately 80 km^2 region. The classification scheme was composed of 12 classes including water, village sites and common vegetation types. Two of the classes were Archaeological Sites Not Under Cultivation and Archaeological Sites Under Cultivation. The high accuracy associated with classifying water bodies, savannah, forest and cultural sites elevated the accuracy of the classification as a whole. For Archaeological Sites Not Under Cultivation and Archaeological Sites Under Cultivation, however, producer accuracies were 78 and 41 percent, respectively. User accuracy for the same classes were 41 and 62 percent.

While Russell's (2005) overall classification was quite accurate, the methods' ability to classify archaeological sites was low. Also, Russell studied sites that were

likely used on a rotational basis, interspersed with fallow periods. It is hoped that using a time-series approach will increase classification accuracy and allow for classifying ADE sites that have been abandoned for much longer periods of time.

The effects of ADE on agricultural vegetation are well understood (Glaser et al. 2001; Major et al. 2005; Schlesinger 1991); however, its effects on forest vegetation are less studied, primarily because there are few known forest ADE sites. Several studies have reported colloquial evidence that ADE can be identified by indicator tree species, which tend to be more exotic and more useful that the species growing on non-ADE (Moran 1981; Sombroek et al. 2002; Woods and McCann 1999) and at least one study has been able to support that evidence empirically (Junqueira 2008). Junqueira established 52 10x25 meter (250 m^2) plots along the middle Madeira River in Amazonas State, Brazil. Twenty-six of these were on ADE soils and 26 were on non-ADE soils. In addition to interviewing local *caboclo* farmers to learn how ADE-based and non-ADE-based forests were used, Junqueira conducted a census of all trees with diameter at breast height (DBH) greater than or equal to 5 cm and all palms taller than 1 meter. An analysis of this data revealed several important findings (Junqueira 2008):

1. ADE sites showed higher density (169 individuals, $p = 0.025$) and higher richness (25 species, $p = 0.06$) of tree species than non-ADE sites (113 individuals, 14 species).

2. Six ADE indicator species (mostly palms) and 3 non-ADE indicator species were identified, which supports the evidence collected during earlier ethnobotanic studies (Moran 1981; Sombroek et al. 2002; Woods and McCann 1999).
3. Despite the different palm species present on ADE, there was no difference in the number of palms growing on ADE verses non-ADE nor was there a difference in palm species richness between the two soil types.
4. The principle difference between vegetation growing on the two soil types is species composition, in both woody plants and palms.
5. A second major difference relates to vegetation structure. In typical tropical forests there is a reduction in woody plant understory density as succession advances and the canopy closes, reducing the amount of light that reaches the sub-canopy. On ADE sites, woody plant density remained high during succession, possibly because the higher soil fertility encourages a greater number of pioneer species with a shorter life cycle. As these individuals die and fall, openings occur in the canopy and more light reaches the sub-canopy allowing for a denser understory (Junqueira 2008). This finding is consistent with those of Laurance et al. (1999) who attribute the decline in biomass on Amazonian secondary forests to poor soil quality (see also de Castilho et al. 2006).

The main driver of vegetation phenology in ever-moist tropical forests is incoming photosynthetically active radiation (PAR, Huete et al. 2002; Myneni et al. 2007; Van Schaik et al. 1993; Wright and Van Schaik 1994; Zimmerman et al. 2007)

rather than soil moisture or precipitation. Henderson et al. (2000) studied the flowering phenologies of palm trees at the Smithsonian Institution/INPA's (Brazil's National Institute of Amazonian Research) Biological Dynamics of Forest Fragments Project (BDFF) located about 41 km north of the present study site. They determined that palms show no preference for wet or dry season flowering as a community, but that individual taxa and species tend to flower in either the wet or dry seasons. Specifically, they report that taxa of the genus *Bactris* – Junqueira (2008) identifies at least one *Bactris* species as an ADE indicator – tend to flower during the rainy season. *Oenocarpus minor* Mart. is an ADE indicator species and it also flowers during the rainy season. Taxa of *Astrocaryum* flower during the dry season and Junqueira identify three members of this genera as non-ADE soil indicator species. One species of *Attalea* and one of *Geonoma*, however, were identified by Junqueira as ADE indicators and these genera tend to flower during the dry season (Henderson et al. 2000). It seems that with a few exceptions, the ADE indicator palm species tend to flower in the rainy season and the non-ADE indicator palm species tend to flower in the dry season.

Hypothesis 1: ADE soils tend to exhibit greater density of woody species than do non-ADE soils. This increased density remains as forest succession progresses, unlike the reduction in density that is typical of Amazonian forests. Enhanced Vegetation Index values (EVI, Huete et al. 2002) and the near-infrared (NIR) bands of NASA's Moderate Resolution Imaging Spectroradiometer (MODIS) sensor have been

shown to be sensitive to vegetation structure (Gao et al. 2000). If the MODIS sensor is sensitive to the different densities of vegetation growing on ADE and on non-ADE then a reliable model for predicting the location of currently unknown ADE sites could be developed.

Hypothesis 2: ADE sites tend to contain different tree species than do non-ADE sites, particularly palm species. If these different species possess different spectral reflectance properties, either consistently throughout the year or during specific times of the year due to different flowering phenologies, then a remote sensing model for predicting the location of unknown ADE sites could be developed. The difficulty with testing this hypothesis is that most of these palm species are a part of the sub-canopy and are therefore occluded by taller woody species. A study conducted 430 km east of the present study site found a slight increase in EVI values during the late dry season, that the authors linked to the phenology of the herbaceous understory (Huete et al. 2002). A similar increase was also identified by Myneni et al. (2007) and Xiao et al. (2006). If this increase is detected in our study site it may contribute to a successful ADE classification method.

3.2 Methodology

3.2.1. Study Site

The study site is a transect that begins in Manaus, Amazonas State, Brazil and runs west-southwest for nearly 400 km (Fig. 1). Petrobras, the Brazilian national

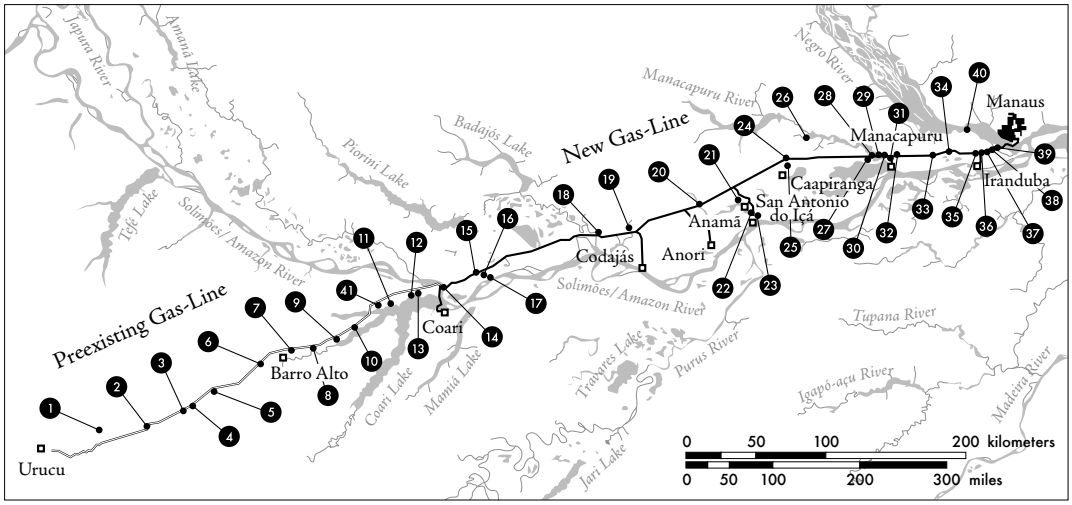

Figure 3.1: Map of the Coari-to-Manaus gas-line. The numbered points are the ADE locations. Source: Neves 2007.

petroleum company, is constructing a gas-line that will connect the city of Coari with the city of Manaus. Once the new line is finished and connected to the existing 285 km line that connects Urucu with Coari, it will transport 4.7-million-m^2 of natural gas to Manaus every day for electric power generation. An additional 125 km of gas-line will be constructed to connect the main line with the municipalities of Coari, Codajás, Anamã, Caapiranga, Manacapuru and Iranduba.

The surveyors for the new gas-line were accompanied by archaeologists from the University of São Paulo, who mapped and assessed the archaeological sites found along the route (Neves et al. 2007). Forty-one new ADE sites were discovered; of these, 28 where found along the new gas-line that was cleared in 2006. Prior to 2006, these ADE sites were covered by forest. The majority of known ADE sites have long ago been cleared of natural vegetation to take advantage of the soil's high fertility for agricultural purposes. These sites have typically been used for generations and under

different land management practices and the dates of clearing and fallow periods are often difficult, if not impossible, to determine. The gas-line dataset uniquely provides the location of ADE sites and the date of clearing so that pre-clearing imagery can be used to assess the effects of ADE on forest vegetation.

Non-ADE sites were selected at random intervals along the transect, at least 2 km from known ADE sites. This ensured that there was no accidental overlap of an ADE site.

3.2.2. Data

Complete annual time-series of Moderate Resolution Imaging Spectroradiometer (MODIS) MOD13Q1 version 005 Enhanced Vegetation Index (EVI)(Huete et al. 2002) imagery for 2001 through 2005 were downloaded from NASA's WIST data gateway website (NASA 2009). MODIS surface reflectance data are processed as 16-day maximum value composite (MVC) EVI data with 250-m spatial resolution. Pre-processing involves correcting for cloud and aerosol contamination as well as angular, Sun-target-sensor variations with an option to use bidirectional reflectance distribution function (BRDF) models. EVI exhibits less saturation in tropical regions than many vegetation indices (Didian 2002), is related to forest stand biomass (Roberts et al. 2003), to tropical forest leaf litterfall (Saleska et al. 2003; Xiao et al. 2005), to leaf canopy processes (Xiao et al. 2005), and is more sensitive to seasonal dynamics than other vegetation indices (Ferreira et al. 2003).

The traditional maximum value compositing (MVC) process selects the highest pixel value as representative of the entire composite period, effectively reducing the effects of cloud interference and aerosol contamination in data that have not been atmospherically corrected (Holben 1986). For data that have been atmospherically corrected prior to being composited (like MODIS) the MVC process tends to select pixels with large view and solar zenith angles, which may not be the most cloud-free pixels (Cihlar et al. 1997; Goward et al. 1991). To correct for this problem, a constrained view angle maximum value composite (CV-MVC) process is used for MODIS VI data where the two highest VI values are compared and the observation with the view angle closest to nadir is selected to represent the composite period (Huete et al. 2002). While this effectively limits cloud contamination in most areas, Huete et al. (2002) found persistent cloud cover and cloud shadows near the Tapajós region of Brazil, which sits at approximately the same longitude as the present study site.

To reduce the effects of any lingering cloud contamination, the time-series data were smoothed prior to analysis using a modification of the mean value iteration (MVI) method introduced by Ma and Veroustraete (2006). MVI first identifies points along the time-series that might be erroneous by comparing their values to the mean of their two neighbors such that if $|(DN_{i-1} + DN_{i+1})/2 - DN_i| >$ threshold, then the value at DN_i is replaced with $(DN_{i-1} + DN_{i+1})/2$, where DN_i is the digital number in the *i*th position within the time-series. This process is repeated until the absolute difference

between every point and the mean of its two neighbors is less than the threshold. This method elevates downward troughs and compresses upward spikes to create a smoothed time-series. Since we were looking at tropical forest presumed to have a slight unimodal annual phenologic cycle (Huete et al. 2002; Van Schaik et al. 1993; Wright and Van Schaik 1994; Zimmerman et al. 2007), downward spikes were assumed to be the result of cloud contamination. The values that sat on the upper envelope were assumed to be accurate EVI values. It is desirable to replace any downward spikes, but retain the upper envelope (Hird and McDermid 2009). To maintain the upper envelope we applied two thresholds, one for identifying

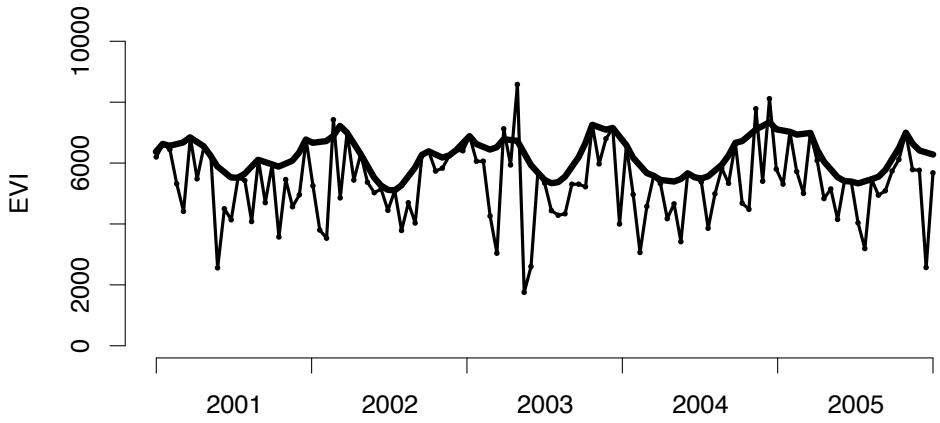

Figure 3.2: Example of an annual EVI time-series before and after smoothing by the modified Mean-Value Iteration method.

downward spikes and one for identifying upward spikes that exceed the envelope. Our thresholds were 100 for locating downward spikes and 2500 for locating upward spikes. This dual-threshold modification of the MVI allowed us to repair spurious negatively biased spikes caused by cloud and aerosol contamination while retaining

the upper envelope of the time-series. Fig. 3.2 shows an example of an EVI time-series before and after modified MVI smoothing.

Of the 41 ADE sites discovered along the gas-line, the first 13 were excluded from the analysis because they were located along the preexisting gas-line, which prevented pure forest pixels from being collected. Also, sites 26, 28 and 39 were excluded because these sites are located along the banks of either the Manacapuru or Negro rivers and at the 250-m resolution of MODIS these pixels contained water reflectance and were not pure vegetation pixels.

3.2.3. Overview of Harmonic Analysis

Harmonic analysis, or Discrete Fourier Analysis, permits a complex curve, such as an annual EVI time-series, to be expressed as the sum of a series of cosine waves (Bloomfield 1976; Broughton and Bryan 2009). Each of the cosine waves is defined by a unique wavelength, phase and amplitude. The wavelength, or harmonic term, designates the number of cycles completed by the time-series over its chronological range. The term of each wave is supplied by the user and the amplitude and phase values are calculated to return the cosine wave that best fits the original time-series. The cosine curves are calculated in order of their respective terms, not in decreasing order of fit to the time-series. The first term cosine function is the best fit curve constrained to a frequency of one, the second term cosine function is the best fit curve constrained to a frequency of two, and so on. Successive harmonic curves are added to produce a more complex curve, approximating the original time-series. The

sum of all possible harmonic curves reproduces the original time-series. The lower order waves demonstrate trends in the data, while the higher order waves contain mostly noise (Jakubauskas et al. 2001).

Harmonic analysis summarizes vegetation dynamics in two values, the amplitude and the phase (Fig. 2.3). The amplitude of the first harmonic indicates the variability of seasonal productivity over the year as expressed in a single pulse of net primary production (NPP). The phase of the first harmonic summarizes the timing of vegetation green-up and senescence (i.e., the start and end of the growing season). Subsequent harmonic values indicate the strength (amplitude) and timing (phase) of higher frequency patterns, such as secondary vegetation types. The additive term of the harmonic series, or the mean value of the time-series, indicates overall productivity. The amplitude and phase of the lower-order harmonics have been used successfully in land cover/land use classification and they work especially well in differentiating vegetation functional groups (Jakubauskas et al. 2001; Jakubauskas et al. 2002; Moody and Johnson 2001).

The equations for amplitude and phase follow (Broughton and Bryan 2009; Jakubauskas et al. 2001):

$$amplitude = \sqrt{C_f(x) + S_f(x)} \quad (1)$$

$$phase = \arctan\left(\frac{C_f(x)}{S_f(x)}\right) \quad (2)$$

If $C_f(x)$ is less than zero then π is added to the phase. The equations for $C_f(x)$ and $S_f(x)$ are:

$$C_f(x) = \sum_{i=1}^{n} \left(i \times \cos\left(\frac{2\pi x f}{n} \right) \right) \times \frac{2}{n} \quad (3)$$

$$S_f(x) = \sum_{i=1}^{n} \left(i \times \sin\left(\frac{2\pi x f}{n} \right) \right) \times \frac{2}{n} \quad (4)$$

Where n is the length of the time-series, i is the data value from the time-series, x is the temporal unit of each i, and f is the term (or frequency) of the harmonic being calculated.

The phase values returned by equation 2 range from zero to 2π and, since they are circular values, a phase of zero is equivalent to a phase of 2π. The phase of the first harmonic indicates the position of the crest of the wave. A phase angle of π indicates that the curve peaks at the center of the time-series, while a phase angle of 2π indicates that the peak occurs at the extremes of the period and the trough of the curve is located at the middle of the time-series.

3.2.4. Use of Harmonic Analysis in Vegetation Studies

One of the most common applications of Harmonic Analysis (HA) is smoothing noisy data (Bradley et al. 2007) and replacing clouded pixels in vegetation index time-series (Jun et al. 2004). Roerink et al. (2003) applied HA to annual time-series of vegetation index values calculated from imagery collected by the Advanced Very High Resolution Radiometer (AVHRR) satellite sensor over Europe and Sahelian Africa. The amplitude value was used as an estimate of annual ecosystem variability. When the amplitude was compared to a climate indicator the driest, warmest areas were found to be the most sensitive to climate variation. Jakubauskas

et al. (2002) used phase angles to estimate variation in inter-annual phenology. Inter-annual landscape variability was estimated by calculating a weighted circular variance of each pixels' multi-year phase angles.

Ollson and Eklundh (1994) used a least-squares fitting procedure to compare a vegetation index time-series to its first and second harmonic curves to determine whether vegetation in Africa exhibited a mono-modal or bi-modal pattern. In this method the harmonic term with the best fit to the original time-series is selected and used to determine the n-modal nature of the time-series. Brown et al. (2007) used a similar method to map agricultural intensification in Vilhena, Brazil. Brown et al. (2007) calculated the amplitudes of the first three harmonic terms and used these data to determine whether pixels represented single-, double-, or triple-cropped agricultural sites. This simple classification scheme mapped agricultural intensification with 80% accuracy.

Morton et al. (2006) calculated several descriptive statistics, including the amplitude and phase values, of MODIS vegetation index time-series collected over Mato Grosso, Brazil. These variables were entered into a decision tree classifier which successfully classified land cover as either cropland, pastureland or re-growth forest.

Lacruz and Sousa (2007) mapped the flood plain of the Taquari River in Brazil using HA and 2005 MODIS vegetation index time-series. They calculated the curve of the first harmonic term and then compared it to the original time-series using

the coefficient of determination. Their study site was a grassland, that has a strong mono-modal seasonal pattern, therefore the coefficient of determination was typically high. In the floodplain, where rising waters disrupt the grasslands' mono-modal pattern, the coefficient of determination was low. They found that the floodplains were clearly identified when the coefficient of determination was equal to or less than 0.20. They were also able to differentiate between farmland and pastureland using amplitude and phase values.

While other methods exist for quantifying vegetation phenology using remotely sensed time-series (Ahl et al. 2006; Duchemin et al. 1999; Zhang et al. 2003), HA is advantageous because it does not rely on thresholds or other moving window methods. This is much more robust in the tropics where differences in seasonal vegetation are very slight.

3.3 Analysis

To test Hypothesis 1, which is that EVI values collected over ADE will not equal those collected over non-ADE due to increased vegetation density and differences in species reflectance values, a Multiple Analysis of Variance (MANOVA) was performed on the annual means of the data for each year. This resulted in 25 observations (site locations) and five variables (annual means) for each soil type. A logistic regression was performed on this data to predict whether each sample site is an ADE location. A jackknife procedure was used as a rough accuracy assessment.

Accuracy scores are reported as the percentage of sites classified correctly as either ADE or non-ADE.

To test Hypothesis 2, which is that EVI values for ADE and non-ADE will vary throughout the year due to the different phenology patterns of their associated species, t-tests were used to compare the two sets of EVI values from each period in the 5-year time-series. More conservative two-tailed t-tests were applied, although there seems to be a tendency for ADE-based vegetation to have lower EVI values. The p-values from the t-tests were graphed to determine at which period of the year the two soil types could be most easily distinguished. Those periods whose t-test p-values were less than $\alpha = 0.01$ were used in a logistic regression to predict whether each sample site is an ADE location. A jackknife procedure was used as a rough accuracy assessment.

In addition to the t-tests, harmonic variables were calculated for each year using equations 1-4. These were entered into a MANOVA with 25 observations and 10 variables (the additive term, and amplitude for each of the five years). The phase angles were not included because they are nonlinear. A logistic regression was used to predict the percentage likelihood of ADE. A jackknife procedure was used as a rough accuracy assessment. Phase angles are circular variables, i.e. 0° equals 360°; therefore, the circular mean and circular variance were calculated for these variables. Circular variance ranges from zero to one; a value of one indicates that the angles are dispersed uniformly around the circle and a value of zero suggests that the angles are

clustered together (Jakubauskas et al. 2002). A circular ANOVA was performed for each year to determine if there was a significant difference between the phase angles associated with ADE and those associated with non-ADE (Mardia and Jupp 1999). All analysis were performed using the R Statistical Environment (R Development Core Team 2008).

3.4 Results

The annual means of EVI values of vegetation growing on ADE and vegetation growing on non-ADE were sufficiently different to reject Null Hypothesis 1 (MANOVA Pillai = 0.262, p = 0.017). Accordingly, we conclude that the canopy density associated with ADE vegetation is significantly different from the vegetation density associated with non-ADE, as measured by MODIS EVI. The means of each years' EVI values for ADE and non-ADE are shown in Fig. 3.3a and their densities are shown in the first row of Fig. 3.4. Only the means of 2003 were significant contributors to the logistic regression (p-value = 0.034). The means of 2005 were nearly significant (p-value = 0.053), but all other years' means were larger than 0.3. This indicates that 2003 may be a uniquely optimal year for mapping ADE using vegetation EVI as a surrogate for soil type. A jackknife procedure on the logistic regression performed on the annual mean EVI data correctly classified ADE and non-ADE sites 66% of the time.

Fig. 3.3a shows that vegetation growing on ADE typically has a lower EVI value than vegetation growing on non-ADE. This relationship is consistent throughout the year, although the dispersion of values around their means is so large that significant overlap occurs between the two datasets. The series of 115 T-tests, one for each of the 23 composite periods in each of the five years, demonstrates that the difference between vegetation growing on ADE and vegetation growing on non-ADE is most significant during the dry season (Fig. 3.3). In this area the dry season occurs from October to June. The results displayed in Fig. 3.3b show that ADE and non-ADE based vegetation is discernible (T-test p-values < 0.05) at roughly the same time-period. The periods of significant p-values seems to precede the dry season and encroach into the wet season slightly. This is likely because atmospheric correction preprocessing is more successful at eliminating the effects of cloud interference when there are fewer clouds in the image. When the wet season is well underway and cloud interference is at its maximum, the preprocessing algorithms are likely unable to correct for all of the contamination, which obscures the difference between vegetation growing on ADE and vegetation growing on non-ADE.

Despite the difference between ADE and non-ADE based vegetation during the dry season, a MANOVA conducted on those composite periods with T-test p-values less than 0.01 did not return a significant result (Pallai = 0.708, p = 0.080). A jackknife procedure on the logistic regression of the composite periods with T-test p-values less than 0.01 returned an accuracy of 56%.

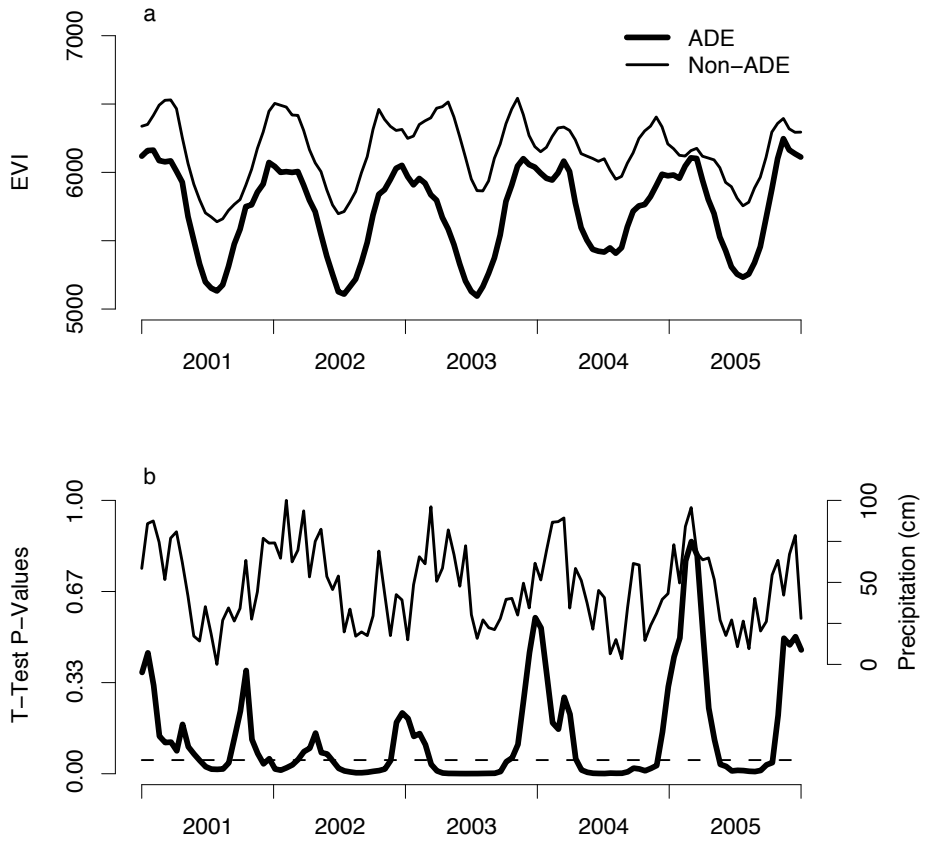

Figure 3.3: The difference between a time-series of EVI collected over ADE and non-ADE; a) shows the composite period mean for the 25 samples, and b) shows p-values from T-tests conducted for each composite period. The precipitation line drawn on b is the mean of data collected at the municipalities of Barro Alto, Anamã, San Antonio do Içã and Caapiranga.

The densities of the harmonic variables are presented in Fig. 3.4 and their means and standard deviations are listed in Table 3.1. The additive term (time-series mean) and the amplitude of the first harmonic were calculated for 2001-2005 and entered into a MANOVA. The results of the MANOVA test were insignificant (Pallai = 0.340, p = 0.059). The jackknifed logistic model of the harmonic variables was able to classify ADE and non-ADE sites correctly 68% of the time.

		2001	2002	2003	2004	2005
ADE	Additive Term	5719.0 ± 800.4	5676.5 ± 846.3	5659.9 ± 861.6	5738.1 ± 739.0	5771.5 ± 796.8
	Amplitude	628.6 ± 335.4	591.3 ± 225.5	665.9 ± 250.0	478.4 ± 282.9	710.3 ± 333.0
	Phase Angles	0.566 ± 0.702	0.426 ± 0.854	0.232 ± 0.936	0.253 ± 1.040	0.235 ± 0.925
Non-ADE	Additive Term	6083 ± 312.6	6161.2 ± 314.3	6259.2 ± 457.8	6184.4 ± 393.3	6092.4 ± 360.7
	Amplitude	603.4 ± 286.1	488.4 ± 220.3	507.5 ± 255.4	437.8 ± 199.2	540.6 ± 226.8
	Phase Angles	0.744 ± 0.824	0.218 ± 0.884	0.479 ± 1.496	0.086 ± 1.509	6.196 ± 1.321

Table 3.1: The descriptive statistics of the Harmonic variables. The mean and standard deviation values for the phase angles are circular means and circular standard deviations.

The harmonic phase angles did not contribute to a successful classification. The circular variance values are located in Table 3.2. While the ADE sites have more concentrated, less dispersed, phase angles than do the non-ADE sites, this difference was not enough to discern between the two soil types. The circular ANOVA p-values for each year were 2001 = 0.424, 2002 = 0.414, 2003 = 0.524, 2004 = 0.618, and 2005 = 0.350.

	2001	2002	2003	2004	2005
ADE	0.218	0.306	0.355	0.418	0.348
Non-ADE	0.288	0.323	0.673	0.68	0.582
ANOVA p-value	0.424	0.414	0.524	0.681	0.35

Table 3.2: The circular variances and p-values from circular ANOVA tests conducted on the harmonic phase angles.

Since the dry season, which occurs between October and June, typically has higher EVI values than the wet season (Huete et al. 2002; Myneni et al. 2007; Van Schaik et al. 1993; Wright and Van Schaik 1994; Zimmerman et al. 2007), we expect the phase angles to cluster near 2π. Phase angles are circular, i.e. 2π equals zero, so the phase angles will either be a little less than 2π or a little larger than zero. Circular

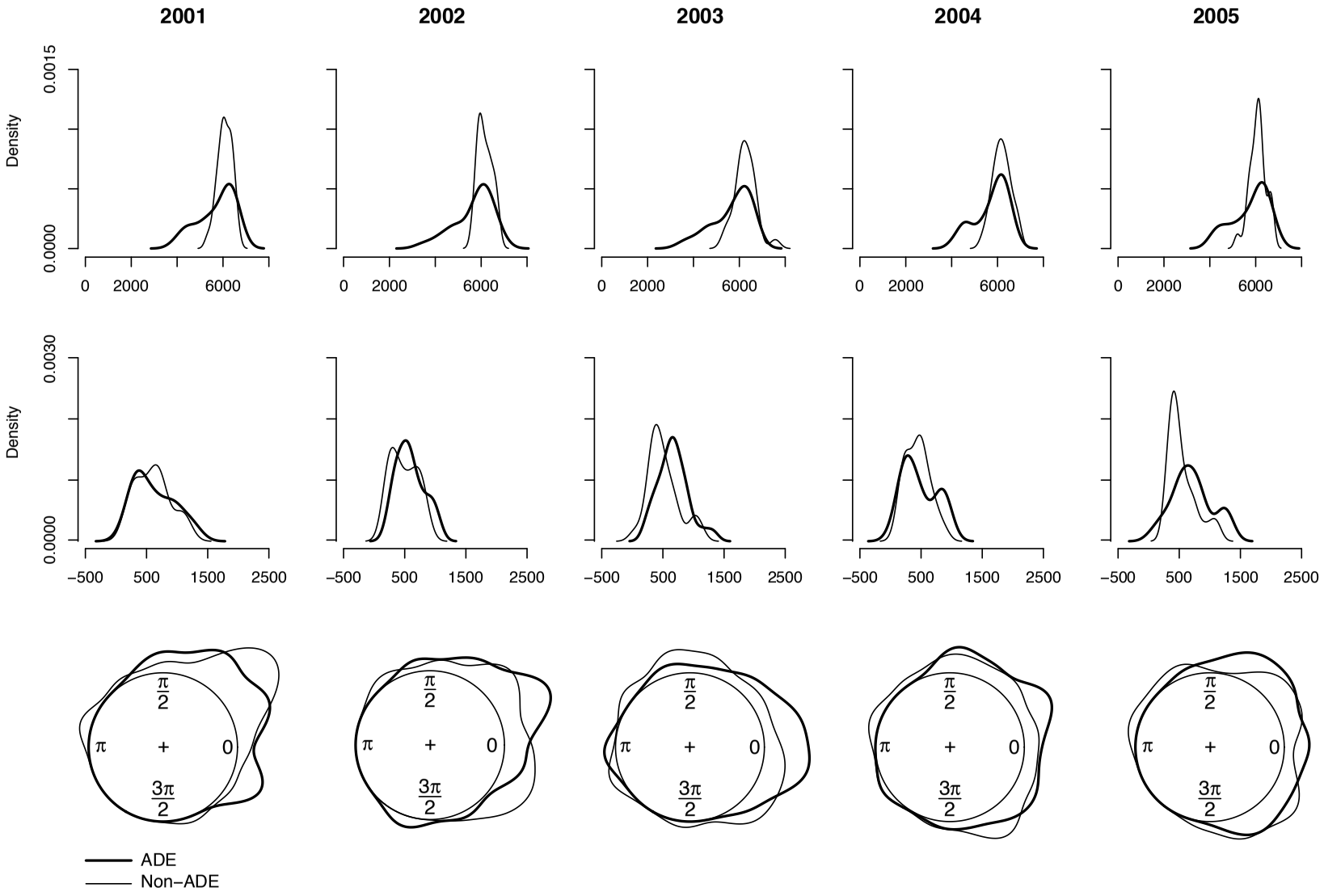

Figure 3.4: Densities of the Harmonic Wave variables for EVI collected from ADE and from non-ADE; a) is the additive term or annual mean, b) is the first harmonic amplitude, and c) is the circular density of the first harmonic phase angles. The thick lines correspond to ADE and the think lines correspond to non-ADE sites.

variance is a measure of how tightly clustered angles are around their circular mean. A circular variance near zero indicates that angles are very tightly clustered, a circular variance of one indicates that the angles are dispersed uniformly in circular space. The annual mean phase angles for ADE are clustered around their mean of 0.35 (circular variance = 0.34). The annual mean phase angles for non-ADE are centered on 0.34, but they are not as tightly clustered (circular variance = 0.53), as expected. This indicates that harmonic phase angles have the potential to provide useful information regarding tropical forest vegetation. Unfortunately, at the spatial and spectral resolution of the MODIS sensor, harmonic phase angles did not provide sufficient information for an accurate classification of ADE and non-ADE soils. This, with the tests discussed above, leads us to fail to reject Null Hypothesis 2.

3.5 Discussion

This study has shown that forest vegetation growing on ADE soils and forest vegetation growing on the surrounding typical Amazonian soils exhibit different spectral characteristics during the dry-season months (Fig. 3.3). While EVI values for the two soil types are statistically indistinguishable during the wet-season, EVI values for the ADE sites in this study drop significantly lower than those of the non-ADE sites. The distribution of EVI values, and their harmonic variables, is so broad that accurate classification of sites into either ADE or non-ADE soil types was not possible using a logistic regression model. Nonetheless, we provide evidence that

2003 may be a uniquely good year for differentiating between ADE and non-ADE based vegetation.

We failed to reject both of our hypotheses. Hypothesis 1 stated that the difference between EVI values collected from vegetation growing on ADE soils and EVI values collected from vegetation growing on non-ADE soils was a result of the higher vegetation density typical of ADE sites. Hypothesis 2 stated that the difference between ADE and non-ADE EVI values could be explained by phenological differences in the different vegetation indicator communities common to ADE and non-ADE sites.

The results from the series of T-tests performed on the composite periods of the 5-year time-series seem promising. Also, the results of the MANOVA test performed on the annual means of the data was significant at the 0.1 alpha level. While this was not sufficient to confidently reject the null hypothesis, it may indicate that imagery with higher spatial resolution may be successful. Perhaps a time-series of satellite imagery with finer spatial resolution will have the detail necessary to make an accurate classification.

Finer spatial resolution would also help eliminate mixed pixels, which were common in this study. The geographic coordinates of the ADE sites used in this study were collected by archaeologists from the University of São Paulo who were concerned only with being able to find the sites again. No effort was made to ensure that GPS points were collected in the center of the ADE patches. We suspect that such

an effort, which would reduce mixed pixels, would result in increased classification accuracy. Also, 80% of known ADE patches are smaller than two hectares (Kern et al. 2003). At the spatial resolution of MODIS (6.5 hectares per pixel) these smaller sites are also mixed pixels. The use of imagery with finer spatial resolution would reduce mixed pixels and could result in better classification accuracy. Russell's (2005) moderate success with Landsat imagery for identifying archaeological sites suggests that this may be the case.

Another source of classification confusion may be the soil moisture capacity of clayey soils in the region. Earlier studies have indicated that ADE soils are better able to retain moisture than non-ADE soils (Lehmann et al. 2003b). However, Teixeira (2008) has found that, even though ADE have slightly higher moisture retention than non-ADE soils with similar microstructure, the increased soil moisture capacity of ADE is primarily a function of its clay content, so that clayey Oxisols and ADE share similar soil moisture capacities. It is likely then, that at least some clayey non-ADE sites may be misclassified as ADE soils.

Based on evidence provided by Junqueira (2008) and Henderson et al. (2000), we had hypothesized that ADE indicator species flower during the rainy season and ,therefore, have different EVI values than the palm species that typically grow on non-ADE soils. It is likely that the understory indicator species were too occluded by the forest canopy and did not have sufficient effect on the spectral reflectances that are used to calculate EVI values. Future attempts to use remotely sensed data to

predict ADE location should focus on the spectral properties of the upper canopy rather than the understory. Unfortunately, the effects of ADE on upper canopy species is less understood that its effects on the understory.

While MODIS based harmonic variables are able to differentiate between cropland, pastureland and forest sites with acceptable accuracy (Brown et al. 2007; Morton et al. 2006), they are inadequate for a highly accurate classification between annual patterns as closely related as vegetation growing on different soil types in the Amazon Basin. Nonetheless, this method allows researchers to find ADE locations nearly seven out of ten tries, which is a tremendous improvement over the success rate of trekking through the forest in the hope of stumbling upon an ADE site. Future research is planned that may improve this accuracy even more.

A model with the ability to accurately predict the location of currently unknown ADE sites would greatly benefit the Amazonian archaeological and biogeographical communities. While this research provided a step in that direction, additional work is necessary to construct a suitable predictive model.

Chapter 4
Review and Final Thoughts

4.1 Review and Conclusions

Amazonian Dark Earths (ADE) are important subjects of study, not only for their obvious value as archaeologic and cultural phenomena, but also for their potential to sequester carbon for millennial time-scales. Before anthropogenic manipulation, these soils were often Amazonian Oxisols, weathered and depleted. The formation of ADE involved the addition of organic matter and charcoal. The charcoal stabilizes the minerals and nutrients in the soil. The charcoal contains more carbon than most soil organic matter and it is very recalcitrant. Charcoal added to the soil over 2,000 years ago is still safely locked away. ADE soils provide a unique opportunity to study the effects and permanency of sequestering carbon in soils.

Research into the properties and value of ADE is limited by the fact that most ADE sites are still hidden beneath the forest canopy. This dissertation attempted to overcome that limitation by developing a satellite image based model for predicting the location of currently unknown ADE sites. Chapter 1 discussed the value and physical characteristics of ADE. Chapter 2 outlined in detail the theory and application of a methodology for locating ADE sites. Chapter 3 discussed the application of that methodology to a study site in Brazil's Amazonas State. Chapter 3 also introduced a data-set of known ADE sites that until 2006 were located under dense forest. There is no record of when these sites were abandoned, but it is safe to

assume that it happened centuries, if not millennia, ago. This is a very unique data-set that deserves additional study.

The most difficult element of this project has been dealing with the extreme density of vegetation in the humid tropics and its lack of a clear growing season. Looking for specific vegetation patterns in the abundance of Amazonian vegetation is more difficult than finding the notorious needle in the haystack – the needle is at least a different color. All the methods and techniques I employed in this project have been successfully used in more temperate locations where vegetation displays more obvious growth patterns. The lushness and fecundity of the vegetation of the Amazon Basin that makes studying it interesting to study also makes it difficult to study.

Although I was unable to produce an effective, accurate model for locating ADE, I did accomplish several goals:

1. I have demonstrated that MODIS data does not have the spatial resolution to locate ADE sites. I had hoped that the superior atmospheric correction of MODIS imagery would compensate for its large pixel size, but this was not the case.
2. I have demonstrated that Harmonic Wave Analysis is nearly able to differentiate between MODIS EVI time-series collected over vegetation growing on ADE and vegetation growing on non-ADE. At the spatial resolution of MODIS, the method was not accurate enough to map ADE;

however, the results indicate that the method is sound and may be successful with higher resolution imagery.

3. I have demonstrated that the phase angles of Harmonic Wave Analysis are easily interpreted as estimates of biophysical phenologic timing. This method is less intuitive than methods used commonly in more temporate locations; however, it is more robust and more easily applied in regions with little seasonal variation such as moist tropical forests.

4.2 Tangential Research

In addition to advancing the efforts to produce accurate large-area maps of ADE, my dissertation work has resulted in other research. These projects grew out of and are tangential to my dissertation research.

4.2.1 Temporal Error Introduced by the Composite Process

In Chapter 2, I briefly discussed the temporal error introduced by the Maximum Value Compositing process (MVC - Holben 1986; Huete et al. 2002). This process selects the highest vegetation index value per pixel from a short time-series of images and assigns that value to a composite image that represents the entire time-series. Since cloud and aerosol contamination tend to lower vegetation index values, the result of the MVC process is a nearly cloud and aerosol free image. Unfortunately, the temporal data has been degraded since the user no longer knows the exact date of the image, only that it fell somewhere within the short time-series. Researchers have

had to rely on untested assumptions regarding image dates to perform phenology studies of satellite time-series.

I studied the effects of MVC introduced temporal error and the effects of these common assumptions on satellite image-based time-series phenology studies. My analysis has been published in the *International Journal of Remote Sensing* (Thayn and Price 2008). In that study, I calculated vegetation phenology metrics for over 2,000 natural vegetation sites in Douglas County, Kansas using the common assumptions regarding dates in satellite composite images and using the actual Julian dates (days since December 31 of the previous year). A comparison of the two sets of metrics revealed that the common assumptions can result in errors of up to 10 days in satellite based phenology date estimates. This is very significant when studying phenologic processes that change at a rate of 2.3 to 5.1 days per decade (Parmesan and Yohe 2003; Root et al. 2003) or 0.3-0.4 days per year (Ahas et al. 2002).

4.2.2 Mapping Floodplains and Seasonal Lakes

After presenting preliminary results of my dissertation work at a workshop in Manaus, Brazil I was approached by Dr. Wenceslau Teixeira, of the Brazilian National Agricultural Research Agency (EMBRAPA), who accurately predicted that the dense vegetation canopy of my study site would keep my research from being successful. He then drew my attention back to my preliminary maps and pointed out that while I had failed to map ADE sites, I had done a very good job of mapping floodplains and seasonal lakes.

I have presented my work to map the floodplains and seasonal lakes of the Solimões/Amazon River at the 2008 annual meeting of the American Society for Photogrammetry and Remote Sensing (ASPRS) and the 2008 annual meeting of the Kansas Academy of Science. The Kansas Academy of Science awarded my presentation the Eugene Dehner Award for first place in the doctoral student category. This work is a collaboration with Dr. Teixeira and is nearly ready for submission to peer-review. I am confident that this work will be submitted to *Remote Sensing of Environment* by the end of the summer of 2009.

4.2.3 Pasture Quality Monitoring

While in Brazil, I met with Dr. Rogerío Perrin of EMBRAPA and we discussed the use of satellite remote sensing to monitor pasture quality and management regimes in the State of Amazonas. He is particularly interested in pastures located north of Manaus and on several of the larger islands in the Solimões/ Amazon River. We were able to visit six pasture sites where we talked with landowners and land managers and collected GPS data. I plan to resume this research when my dissertation work is finished.

4.3 Future Research

The primary factor that limited the success of the present research is scale. The typical ADE patch is small, over 80% of them are less than two hectares (Kern et al. 2003) while MODIS pixels encompass 6.25 hectares. Despite this obvious

limitation of MODIS imagery, it was selected for this project because of its superior atmospheric corrections and its ability to generate a nearly cloud free time-series of data. Cloud contamination has historically been a limiting factor in satellite-based remote sensing projects in the Amazon Basin. Satellite sensors with finer spatial resolution do not pass overhead as frequently and are therefore unable to produce as dense a time-series of nearly cloud free images. I had hoped that the increased temporal coverage of MODIS would allow me to locate at least the larger ADE sites, which can be as large as 300 hectares or more.

The archaeology students who collected the GPS points used in this project were concerned only with being able to find the ADE site again. No effort was made to place the coordinates in the center of the patch. This, combined with the large pixel footprint of the MODIS data, practically ensures that each pixel in my training data is a mixed pixel containing some ADE soil and some non-ADE soil. Using imagery with a finer spatial resolution would help alleviate this problem.

Using satellite imagery with a finer spatial resolution would allow me to use Junqueira's dataset (2008). Junqueria conducted extensive tree censuses on ADE and on non-ADE soils located along the middle section of the Madeira River in Brazil. His thesis, which I discuss in detail in Chapter 3, is the first to document the differences in ADE-based vegetation empirically. As part of this census, Junqueira collected GPS data in the center of each of his 52 study sites, which, together with the finer spatial resolution of LandSat should eliminate most mixed pixels. Junqueira

collected copious vegetation biophysical variables as part of his census, which will facilitate model development. The only disadvantage of this data-set is that the ADE sites are used on a rotational basis by local indigenous residents, rather than being completely abandoned.

This dissertation indicates that parts of the methodology employed are sound. The next step in this research is to repeat the analysis using LandSat imagery (0.09 hectares per pixel). I will use both the gas-line dataset (which is the only known dataset of completely abandoned ADE sites) and Junqueira's dataset (which has a wonderful collection of plant biophysical variables collected on semi-managed ADE sites). The difficulty in this next step will be dealing with imagery that contains significant amounts of cloud and aerosol contamination. A careful application of a time-series smoothing algorithm, designed to retain useful vegetation index values by retaining the upper envelope of the time-series, should help with this problem (Hird and McDermid 2009).

4.4 Final Thoughts

I am pleased with the results of this study. I have been able to improve researchers' ability to locate ADE sites hidden under tropical forest to seven out of 10 attempts. This is much higher accuracy then would be experienced by searching the forest on foot in the hope of stumbling onto an unknown site. This is the first attempt to map ADE sites using satellite remote sensing; however, it builds on previous work

and successfully moves science one step closer to eventually being able to produce an highly accurate map of ADE sites. Most significant science is the result of many researchers working independently toward the same goal, each advancing the work of the others. I have contributed to the effort to map ADE soils and I will continue to contribute to that effort.

Cumulative Bibliography

Ahas, R., Aasa, A., Menzal, A., Fedotova, V.G., & Scheifinger, H. (2002). Changes in European spring phenology. *International Journal of Climatology, 22*, 1727-1738

Ahl, D.E., Gower, S.T., Burrows, S.N., Shabanov, N.V., Myneni, R.B., & Knyazikhin, Y. (2006). Monitoring spring canopy phenology of a deciduous broadleaf forest using MODIS. *Remote Sensing of Environment, 104*, 88-95

Asner, G.P., Bustamante, M.M.C., & Townsend, A.R. (2003). Scale dependence of biophysical structure in deforested areas bordering the Tapajós National Forest, Central Amazon. *Remote Sensing of Environment, 87*, 507-520

Bloomfield, P. (1976). *Fourier Analysis of Time Series: An Introduction*. New York, NY: John Wiley & Sons

Bradley, B.A., Jacob, R.W., Hermance, J.F., & Mustard, J.F. (2007). A curve fitting procedure to derive inter-annual phenologies from time series of noisy satellite NDVI data. *Remote Sensing of Environment, 106*, 137-145

Brondizio, E., Moran, E., Mausel, P., & Wu, Y. (1996). Land cover in the Amazon estuary: Linking of the Thematic Mapper with botanical and historical data. *Photogrammetric Engineering and Remote Sensing, 62*, 921-929

Broughton, S.A., & Bryan, K. (2009). *Discrete Fourier Analysis and Wavelets: Applications to Signal and Image Processing*. Hoboken, New Jersey: John Wiley & Sons, Inc.

Brown, J.C., Jepson, W.E., Kastens, J.H., Lomas, J.M., & Price, K.P. (2007). Multitemporal, moderate-spatial-resolution remote sensing of modern agricultural production and land modification in the Brazilian Amazon. *GIScience and Remote Sensing, 44*, 117-148

Cardille, J.A., & Foley, J.A. (2003). Agricultural land-use change in Brazilian Amazônia between 1940 and 1995: Evidence from integrated satellite and census data. *Remote Sensing of Environment, 87*, 551-562

Carvajal, G. (1934). Discovery of the Orellana River, pp. 167-242. *In* H.D. Heaton (ed.). The Discovery of the Amazon River According to the Account of Friar Gaspar de Carvajal and other Documents, with an Introduction by José Toribio Medina. American Geographical Society Publication 17. New York.

Cihlar, J., Ly, H., Li, Z., Chen, J., Pokrant, H., & Huang, F. (1997). Multi-temporal, multichannel, AVHRR data sets for land biosphere studies: artifacts and corrections. *Remote Sensing of Environment, 60*, 35-57

Costa, M.P.F. (2004). Use of SAR satellites for mapping zonation of vegetation communities in the Amazon floodplain. *International Journal of Remote Sensing, 25*, 1817-1835

Cross, A.M., Settle, J.J., Drake, N.A., & Paivinen, R.T.M. (1991). Subpixel measurement of tropical forest cover using AVHRR data. *International Journal of Remote Sensing, 12*, 1119-1129

de Angelis, C., McGregor, G., & Kidd, C. (2004a). A 3 year climatology of rainfall characteristics over tropical and subtropical South America based on Tropical Rainfall Measuring Mission precipitation radar data. *International Journal of Climatology, 24*, 385-399

de Angelis, C., McGregor, G., & Kidd, C. (2004b). Diurnal cycle of rainfall over the Brazilian Amazon. *Climate Research, 26*, 139-149

de Castilho, C.V., Magnusson, W.E., de Araujo, R.N.O., Luizao, R.C.C., Luizao, F.J., Lima, A.P., & Higuchi, N. (2006). Variation in aboveground tree live biomass in a central Amazonian Forest: Effects of soil and topography. *Forest Ecology and Management, 234*, 85-96

Deneven, W.M. (1992). Stone vs. metal axes: The ambiguity of shifting cultiation in prehistoric Amazonia. *Journal of the Steward Anthropological Society*. 20, 153-165

Dennison, P.E., Roberts, D.A., Peterson, S.H., & Rechel, J. (2005). Use of normalized difference water index for monitoring live fuel moisture. *International Journal of Remote Sensing, 26*, 1035-1042

Didian, K. (2002). MODIS Vegetation Index Production Algorithms. In, *MODIS Outreach on MODIS Vegetation Variables (VI/LAI/FPAR/NPP)*. University of Montana, Missoula, MT

Duchemin, B., Goubier, J., & Courrier, G. (1999). Monitoring phenological key stages and cycle duration of temperate deciduous forest ecosystems with NOAA/AVHRR data. *Remote Sensing of Environment, 67*, 68-82

Ferreira, L., Yoshioka, H., Huete, A., & Sano, E. (2003). Seasonal landscape and spectral vegetation index dynamics in the Brazilian Cerrado: an analysis within the Large-Scale Biosphere-Atmosphere Experiment in Amazônia (LBA). *Remote Sensing of Environment, 87*, 534-550

Gao, X., Huete, A., Ni, W., & Miura, T. (2000). Optical-biophysical relationships of vegetation spectra without background contamination. *Remote Sensing of Environment, 74*, 609-620

Glaser, B. (1999). *Eigenschaften und Stabilität des Humuskörpers der Indianer-schwarzerden Amazoniens*: Bayreuther Bodenkundliche Berichte

Glaser, B., Guggenberger, G., & Zech, W. (2001). The Terra Preta phenomonon: a model for sustainable agriculture in the humid tropics. *Naturwissenschaften, 88*, 37-41

Glaser, B., Guggenberger, G., & Zech, W. (2003a). Organic chemistry studies on Amazonian Dark Earths. In J. Lehmann, D. Kern, B. Glaser & W.I. Woods (Eds.), *Amazonian Dark Earths: Origin, Properties, Management* (pp. 227-241). Netherlands: Kluwer Academic Publishers

Glaser, B., Guggenberger, G., Zech, W., & Ruivo, M.d.L. (2003b). Soil organic matter stability in Amazonian Dark Earths. In J. Lehmann, D. Kern, B. Glaser & W.I. Woods (Eds.), *Amazonian Dark Earths: Origin, Properties, Management* (pp. 141-158). Netherlands: Kluwer Academic Publishers

Glaser, B., & Woods, W.I. (2004). *Amazonian Dark Earths: Explorations in space and time*. Berlin: Springer-Verlag

Goward, S.N., Markham, B., Dye, D.G., Dulaney, W., & Yang, J. (1991). Normalized difference vegetation index measurements for the Advanced Very High Resolution Radiometer. *Remote Sensing of Environment, 35*, 257-277

Hartt, C.F. (1885). Contribução para a ethnologia do Valle do Amazonas II. Taperinha e os sitios dos moradores dos altos. *Archivos do Museu Nacional do Rio de Janeiro, 6*, 10-14

Heckenberger, M.J., Kuikuro, A., Kuikuro, U.T., Russell, J.C., Schmidt, M., Fausto, C., & Franchetto, B. (2003). Amazonia 1492: Pristine forest or cultural parkland. *Science, 301*, 1710-1714

Heckenberger, M.J., Peterson, J.B., & Neves, E.G. (1999). Village size and permanence in Amazonia; two archaeological examples from Brazil. *Latin American Antiquity, 10*, 353-376

Henderson, A., Fischer, B., Scarior, A., Pacheco, M.A.W., & Pardini, R. (2000). Flowering phenology of a palm community in a Central Amazon forest. *Brittonia, 52*, 149-159

Hill, M.J., & Donald, G.E. (2003). Estimating spatio-temporal patterns of agricultural productivity in fragmented landscapes using AVHRR NDVI time series. *Remote Sensing of Environment, 84*, 367-384

Hird, J.N., & McDermid, G.J. (2009). Noise reduction of NDVI time series: An emperical comparison of selected techniques. *Remote Sensing of Environment, 113*, 248-258

Holben, B.N. (1986). Characteristics of maximum value composite images from temporal AVHRR data. *International Journal of Remote Sensing, 7*, 1417-1434

Huete, A., Didan, K., Miura, T., Rodrigues, E.P., Gao, X., & Ferreira, L.G. (2002). Overview of the radiometric and biophysical performance of the MODIS vegetation indices. *Remote Sensing of Environment, 83*, 195-213

Huete, A., Didan, K., Shimabukuro, Y.E., Ratana, P., Saleska, S., Hutya, L., Yang, W., Nemani, R.R., & Myneni, R. (2006). Amazon rainforests green-up with sunlight in dry season. *Geophysical Research Letters, 33*, L06405

Jakubauskas, M.E., Legates, D.R., & Kastens, J.H. (2001). Harmonic analysis of time-series AVHRR NDVI data. *Photogrammetric Engineering and Remote Sensing, 67*, 461-470

Jakubauskas, M.E., Peterson, D., & Kastens, J.H. (2002). Time series remote sensing of landscape-vegetation interactions in the southern Great Plains. *Photogrammetric Engineering and Remote Sensing, 68*, 1021-1030

Jensen, J.R. (2005). *Introductory Digital Image Processing*. Upper Saddle River, NJ

Jipp, P.H., Nepstad, D., Cassel, D.K., & de Carvalho, C.R. (1998). Deep soil moisture storage and transpiration in forests and pastures of seasonally-dry Amazonia. *Climatic Change, 39*, 395-412

Jobbágy, E.G., & Jackson, R.B. (2000). The vertical distribution of soil organic carbon and its relative to climate and vegetation. *Ecological Applications, 10*, 423-436

Jun, W., & Zhongbo, S. (2004). An analytical algorithm of the determination of vegetation Leaf Area Index from TRMM/TMI data. *International Journal of Remote Sensing, 25*, 1223-1234

Jun, W., Zhongbo, S., & Yaoming, M. (2004). Reconstruction of a cloud-free vegetation index time series for the Tibetan plateau. *Mountain Research and Development, 24*, 348-353

Junqueira, A.B. (2008). Uso e manejo da vegetação secundária sobre *Terra Preta* por comunidades tradicionais na região do médio Rio Maderia, Amazonas, Brasil. In, *Programa Integrado de Pós-Graduação em Biologia Tropical e Recursos Naturais* (p. 126). Manaus, Brazil: INPA/UFAM

Kämpf, N., Woods, W.I., Sombroek, W., Kern, D., & Cunha, T.J.K. (2003). Classification of Amazonian Dark Earths and other ancient anthropic soils. In J. Lehmann, D. Kern, B. Glaser & W.I. Woods (Eds.), *Amazonian Dark Earths: Origin, Properties, Management* (pp. 29-50). Netherlands: Kluwer Academic Publishers

Kern, D., D'Aquino, G., Rodrigues, T., Frazão, F.J.L., Sombroek, W., Myers, T.P., & Neves, E.G. (2003). Distribution of Amazonian Dark Earths in the Brazilian Amazon. In C.L. Lehman, D. Kern, B. Glaser & W.I. Woods (Eds.), *Amazonian Dark Earths: Origin, Properties, Management* (pp. 51-75). Netherlands: Kluwer Academic Publishers

Kimes, D., Nelson, R., Skole, D., & Salas, W. (1998). Accuracies in mapping secondary tropical forest age from sequential satellite imagery. *Remote Sensing of Environment, 65*, 112-120

Klassen, J., & McDermid, G. (2007). Remote Sensing of Vegetation: Smoothing Strategies for NDVI Time Series. In, *ASPRS Annual Conference*. Tampa, Florida

Lacruz, M.S.P., & Sousa, M.d.A.J. (2007). Uso de séries temporais EVI/MODIS e análise harmônica para o estudo da bacia do rio Taquari. *Revista Brasileira de Cartografia, 59*, 9-15

Laurance, W.F., Laurance, S.G., Delamonica, P., Rankin-De Merona, J.M., Gascon, C., Fearnside, P.M., Lovejoy, T.E., & Chambers, J.Q. (1999). Relationship between soils and Amazon forest biomass: A landscape-scale study. *Forest Ecology and Management, 118*, 127-138

Lehmann, J. (2007). A handful of carbon. *Nature, 447*, 143-144

Lehmann, J., da Silva Jr., J.P., Steiner, C., Nehls, T., Zech, W., & Glaser, B. (2003a). Nutrient availability and leaching in an archaeological Anthrosol and a Ferrasol in the Central Amazon basin: fertilizer, manure and charcoal amendments. *Plant and Soil, 249*, 343-357

Lehmann, J., Gaunt, J., & Rondon, M. (2006). Bio-char sequestration in terrestrial ecosystems–A review. *Mitigation and Adaptation Strategies for Global Change*, 403-427

Lehmann, J., Kern, D., German, L., McCann, J.M., Martines, G.C., & Moriera, A. (2003b). Soil fertility and production potential. In J. Lehmann, D. Kern, B. Glaser & W.I. Woods (Eds.), *Amazonian Dark Earths: Origin, Properties, Management* (pp. 105-124). Netherlands: Kluwer Academic Publishers

Lehmann, J. & Stephen, J. (Eds.) (2009). *Biochar for Environmental Management.* Earthscan, London

Lu, D., Batistella, M., Moran, E., & Mausel, P. (2004a). Application of spectral mixture analysis to Amazonian land-use and land-cover classification. *International Journal of Remote Sensing, 25*, 5345-5358

Lu, D., Mausel, P., Batistella, M., & Moran, E. (2004b). Comparison of land-cover classification methods in the Brazilian Amazon Basin. *Photogrammetric Engineering and Remote Sensing, 70*, 723-731

Lu, D., Mausel, P., Brondizio, E., & Moran, E. (2004c). Relationships between forest stand parameters and Landsat TM spectral responses in the Brazilian Amazon Basin. *Forest Ecology and Management, 198*, 149-167

Lu, D., Moran, E., & Batistella, M. (2003). Linear mixture model applied to Amazonian vegetation classification. *Remote Sensing of Environment, 87*, 456-469

Lukesch, A. (1976). *The Bearded Indians of the Tropical Forest: The Asuriní of the Ipiaçaba*. Graz, Austria: Akademische Druck -u. Verlagsanstalt

Ma, M., & Veroustraete, F. (2006). Reconstructing pathfinder AVHRR land NDVI time-series data for the Northwest of China. *Advances in Space Research, 37*, 835-840

McCann, J.M. (2002). The Forgotten people of Amazonia. *Science, 297*, 921

Major, J., DiTommaso, A., Lehmann, J., & Falção, N.P.d.S. (2005). Weed dynamics on Amazonian Dark Earth and adjacent soils of Brazil. *Agriculture, Ecosystems and Environment, 111*, 1-12

Malingreau, J.-P., & Tucker, C. (1988). Large-scale deforestation in the southeastern Amazon Basin of Brazil. *Ambio, 17*, 49-55

Mann, C.C. (2002). The real dirt on rainforest fertility. *Science, 297*, 920-922

Mann, C.C. (2005). *1491, New Revelations of the Americas Before Columbus*. New York: Alfred A. Knopf

Mardia, K., & Jupp, P. (1999). Section 7.4. *Directional Statistics*. England: John Wiley and Sons

Marris, E. (2006). Black is the new green. *Nature, 442*, 624-626

McCann, J.M., Woods, W.I., & Meyer, D.W. (2001). Organic Matter and Anthrosols in Amazonia: Interpreting the Amerindian Legacy. In R.M. Rees, B.C. Ball, C.D. Campbell & C.A. Watson (Eds.), *Sustainable Management of Soil Organic Matter* (pp. 180-188)

Meddens, A.J.H. (2006). Possibilities of mapping Amazonian Dark Earths using remote sensing techniques In, *Capita Selecta GIS and Remote Sensing*: Wageningen University

Meggers, B.J. (1992). Prehistoric Population Density in Amazonia. In J.W. Verano & D.H. Ubelaker (Eds.), *Disease and Demography in the Americas* (pp. 172-205). Washington, D.C.: Smithsonian Institution Press

Meggers, B.J. (2001). The continuing quest for El Dorado: Round two. *Latin American Antiquity, 12*, 304-325

Meggers, B.J., Dias, O.F., Miller, E.T., & Perota, C. (1988). Implications of Archaeological Distributions in Amazonia. In W.R. Heyer & P.E. Vanzolini (Eds.), *Proceedings of a Workshop on Neotropical Distribution Patterns* (pp. 275-294). Rio de Janeiro: Academia Brasileira de Ciencias

Moody, A., & Johnson, D. (2001). Land-surface phenologies from AVHRR using the descrete fourier transform. *Remote Sensing of Environment, 57*, 305-323

Mora, S., Herrera, L., Cavelier, I., & Rodrigues, C. (1991). *Cultivars, Anthropic Soils and Stability: a preliminary report of archaeological research in Araracuara, Colombian Amazonia*. Pittsburgh: University of Pittsburgh Latin American Archaeological Reports nº 2

Moran, E.F. (1981). *Developing the Amazon*: Indiana University Press

Morton, D.C., DeFries, R.S., Shimabukuro, Y.E., Anderson, L.O., Arai, E., del Bon Espirito-Santo, F., Freitas, R., & Morisette, J. (2006). Cropland expansion changes deforestation dynamics in the southern Brazilian Amazon. *Proceedings of the National Academy of Sciences of the United States of America, 103*, 14637-14641

Myneni, R., Yang, W., Nemani, R.R., Huete, A., Dickinson, R.E., Knyazikhin, Y., Didan, K., Fu, R., Juárez, R.I.N., Saatchi, S.S., Hashimoto, H., Ichii, K., Shabanov, N.V., Tan, B., Ratana, P., Privette, J.L., Morisette, J., Vermote, E.F., Roy, D.P., Wolfe, R.E., Friedl, M.A., Running, S.W., Votava, P., El-Saleous, N., Devadiga, S., Su, Y., & Salomonson, V.V. (2007). Large seasonal swings in leaf area of Amazon rainforests. *Proceedings of the National Academy of Sciences of the United States of America, 104*, 4820-4823

NASA (2009). NASA WIST Earth Observing System Clearinghouse (ECHO). https://wist.echo.nasa.gov/api/

Nelson, R.F., & Holben, B.N. (1986). Identifying deforestation in Brazil using multiresolution satellite data. *International Journal of Remote Sensing, 7*, 429-448

Nelson, R.F., Horning, N., & Stone, T., A. (1987). Determining the rate of forest conversion in Mato Grosso, Brazil, using Landsat MSS and AVHRR data. *International Journal of Remote Sensing, 8*, 1767-1784

Nepstad, D., de Carvalho, C.R., Davidson, E.A., Jipp, P.H., Lefebvre, P., Negreiros, G.H., da Silva, E.D., Stone, T., A., Trumbore, S.E., & Vieira, S. (1994). The role of deep roots in the hydrological and carbon cycles of Amazonian forests and pastures. *Nature, 372*, 666-669

Nepstad, D., Moutinho, P., Dias-Filho, M., Davidson, E.A., Cardinot, G., Markewitz, D., Figueiredo, R., Vianna, N., Chambers, J.Q., Ray, D., Guerrero, J.B., Lefebvre, P., Sternberg, L., Moreira, M., Barros, L., Ishida, F., Tohlver, I., Belk, E., Kalif, K., & Schwalbe, K. (2002). The effects of partial throughfall exclusion on canopy processes, aboveground production, and biogeochemistry of an Amazon forest. *Journal of Geophysical Research, 107*

Neves, E.G., Da Silva, C.A., Lima, H.P., Carneiro, C.G., & Sampaio, A. (2007). Levantamento arqueológico do gasoduto Coari-Manaus: segundo relatório parcial, levantamento das clareiras, da pista e resultados preliminares das escavaçãoes. In (p. 42)

Neves, E.G., Peterson, J.B., Bartone, R.N., & Da Silva, C.A. (2003). Historical and socio-cultural origins of Amazonian Dark Earths. In J. Lehmann, D. Kern, B. Glaser & W.I. Woods (Eds.), *Amazonian Dark Earths: Origin, Properties, Management* (pp. 29-50). Netherlands: Kluwer Academic Publishers

Oindo, B.O. (2002). Predicting mammal species richness and abundance using multitemporal NDVI. *Photogrammetric Engineering and Remote Sensing, 68*, 623-629

Oliver, J. (2001). The archaeology of forest foraging and agricultural production in Amazonia. In C. McEwan, C. Barreto & E.G. Neves (Eds.), *Unknown Amazon, Culture in Nature in Ancient Brazil* (pp. 50-85). London: British Museum Press

Olsson, L., & Eklundh, L. (1994). Fourier series for analysis of temporal sequences of satellite sensor imagery. *International Journal of Remote Sensing, 15*, 3735-3741

Parmesan, C., & Yohe, G. (2003). A globally coherent fingerprint of climate change impacts across natural systems. *Nature, 421*, 37-42

R Development Core Team (2008). R: A language and environment for statistical computing. In. Vienna, Austria: R Foundation for Statistical Computing

Reed, B.C., Brown, J.F., VanderZee, D., Loveland, T.R., Merchant, J.W., & Ohlen, D.O. (1994). Measuring phenological variability from satellite imagery. *Journal of Vegetation Science, 5*, 703-714

Reed, B.C., White, M., & Brown, J.F. (2003). Remote Sensing Phenology. In Schwartz (Ed.), *Phenology: An Integrative Environmental Science*. Netherlands: Kluwer Academic Publishers

Roberts, D.A., Keller, M., & Soares, J.V. (2003). Studies of land-cover, land-use, and biophysical properties of vegetation in the Large Scale Biosphere Atmosphere experiment in Amazônia. *Remote Sensing of Environment, 87*, 377-388

Roerink, G., Menenti, M., & Soepboer, W. (2003). Assessment of climate impact on vegetation dynamics by using remote sensing. *Physics and Chemistry of the Earth, 28*, 103-109

Roosevelt, A.C., da Costa, M.L., Lopes Machado, C., Michab, M., Mercier, N., Valladas, H., Feathers, J., Barnett, W., da Silveira, M.I., Henderson, A., Sliva, J., Chernoff, B., Reese, D.S., Holman, J.A., Toth, N., & Schick, K. (1996). Paleoindian cave dwellers in the Amazon: the peopling of the Americas. *Science, 272*, 373-384

Root, T.L., Price, J.T., Hall, K.R., Schneider, S.H., Rosenzweig, C., & Pounds, J.A. (2003). Fingerprints of global warming on wild animals and plants. *Nature, 421*, 57-60

Rosenquist, B.R., Forsberg, B.R., Pimentel, T., Rauset, Y.A., & Richey, J.E. (2002). The use of spaceborne radar data to model inundation patterns and trace gas emissions in the central Amazon floodplain. *International Journal of Remote Sensing, 23*, 1303-1328

Rouse, J.W., Haas, R.H., Schell, J.A., & Deering, D.W. (1973). Monitoring vegetation systems in the great plains with ERTS. In, *Third Earth Resources Technology Satellite-1 Symposium* (pp. 309-317). Greenbelt, MD: NASA

Russell, J.C. (2005). Integrated approach to predictive modeling: A case study from the Upper Xingu (Matto Grosso, Brazil). Doctoral Dissertation in Anthropology: University of Florida

Russell, J.C. (2009). Personal telephone conversation

Saatchi, S.S., Nelson, B., Podest, E., & Holt, J. (2000). Mapping land cover types in the Amazon Basin using 1 km JERS-1 mosaic. *International Journal of Remote Sensing, 21*, 1201-1234

Saleska, S., Miller, S., Matross, D., Goulden, M., Wofsy, S., da Rocha, H., de Carmargo, M., Crill, P., Daube, B., de Freitas, H., Hutya, L., Keller, M.E., Kirchhoff, V., Menton, M., Munger, J., Pyle, E., Rice, A., & Silva, H. (2003). Carbon in amazon forests; Unexpected seasonal fluxes and disturbance-induced losses. *Science, 60*, 315-355

Salovaara, K.J., Cárdenas, G.G., & Tuomisto, H. (2004). Forest classification in an Amazonian rainforest landscape using pteridophytes as indicator species. *Ecography, 27*, 689-700

Salovaara, K.J., Thessler, S., Malik, R.N., & Tuomisto, H. (2005). Classification of Amazonian primary rain forest vegetation using Landsat ETM+ satellite imagery. *Remote Sensing of Environment, 97*, 39-51

Santos, J.R., Freitas, C.C., Araujo, L.S., Dutra, L.V., Mura, J.C., Gama, F.F., Soler, L.S., & Sant'Anna, S., J.S. (2003). Airborne P-band SAR applied to aboveground biomass studies in the Brazilian tropical rainforest. *Remote Sensing of Environment, 87*, 482-493

Schlesinger, W.H. (1991). *Biogeochemistry: An analysis of global change*. San Diego: Academic Press

Shilong, P., Jingyun, F., Wei, J., Qinghua, G., Jinhu, K., & Shu, T. (2004). Variation in a satellite-based vegetation index in relation to climate in China. *Journal of Vegetation Science, 15*, 219-226

Silva, B.N.R., Araujo, J.V., Rodrigues, T.E., Falesi, C.I., & Rego, R.S. (1970). *Os solos da área de Cacau Pirera-Manacapuru*

Skole, D., & Tucker, C. (1993). Tropical deforestation and habitat fragmentation in the Amazon: satellite data from 1978 to 1988. *Science, 260*, 1905-1910

Smith, A. (1994). *Explorers of the Amazon*. Chicago: University of Chicago Press

Sombroek, W. (1966). *Amazon Soil: A Reconnaissance of the Soils of the Brazilian Amazon Region*. Wageningen: Centre for Agricultural Publications and Documentation

Sombroek, W., Kern, D., Rodrigues, T., Cravo, M.d.S., Jarbas, T.C., Woods, W.I., & Glaser, B. (2002). Terra Preta and Terra Mulata: pre-Columbian Amazon kitchen middens and agricultural fields, their sustainability and their replication. In, *17th WCSS* (pp. 1935-1931--1935-1939). Thailand

Steere, J.B. (1927). The archaeology of the Amazon. *University of Michigan Official Publication, 29*, 20-26

Steiner, C., Teixeira, W.G., Lehmann, J., Nehls, T., Vasconcelos de Macêdo, J.L., Blum, W.E.H., & Zech, W. (2007). Long term effects of manure, charcoal and mineral fertilization on crop production and fertility on a highly weathered Central Amazonian upland soil. *Plant and Soil*

Steininger, M. (2000). Satellite estimation of tropical secondary forest above-ground biomass: data from Brazil and Bolivia. *International Journal of Remote Sensing, 21*, 1139-1157

Teixeira, M.J. (2008). Personal Communication.

Teixeira, W.G., & Martins, G.C. (2003). Soil physical characterization. In J. Lehmann, D. Kern, B. Glaser & W.I. Woods (Eds.), *Amazonian Dark Earths: Origin, Properties, Management* (pp. 271-286). Netherlands: Kluwer Academic Publishers

Thayn, J.B., & Price, K.P. (2008). Julian dates and introduced temporal error in remote sensing vegetation phenology studies. *International Journal of Remote Sensing, 29*, 6045-6049

Thayn, J.B., Price, K.P., & Woods, W.I. (2008). Locating Amazonian Dark Earths (ADE) using satellite remote sensing – a possible approach. In W.I. Woods, W.G. Teixeira, J. Lehmann, C. Steiner, A. WinklerPrins & L. Rebellato (Eds.), *Amazonain Dark Earths: Wim Sombroek's Vision*. Berlin: Springer-Verlag

Tiessen, H., Cuevas, E., & Chacon, P. (1994). The role of soil organic matter in sustaining soil fertility. *Nature, 371*, 783-785

Van Schaik, C., Terbough, J., & Wright, S. (1993). The phenology of tropical forests-adaptive significance and consequences for primary consumers. *Annual Review of Ecology and Systematics, 24*, 353-377

Velleman, P.F. (1980). Definition and comparison of robust nonlinear data smoothing algorithms. *Journal of the American Statistical Association, 75*, 609-615

Vieira, I.C., Silva de Almeida, A., Davison, E.A., Stone, T., A., Ries de Carvalho, C.J., & Guerrero, J.B. (2003). Classifying successional forests using Landsat spectral properties and ecological characteristics in eastern Amazônia. *Remote Sensing of Environment, 87*, 470-481

Wang, J., Rich, P.M., Price, K.P., & Kettle, W.D. (2004). Relations between NDVI and tree productivity in the central Great Plains. *International Journal of Remote Sensing, 25*, 3127-3138

Wardlow, B.D., Kastens, J.H., & Egbert, S.L. (2006). Using USDA crop progress data for the evaluation of greenup onset date calculated from MODIS 250-meter data. *Photogrammetric Engineering and Remote Sensing, 72*, 1225-1234

Wessels, K.J., de Fries, R.S., Dempewolf, J., Anderson, L.O., Hansen, A.J., Powell, S.L., & Moran, E. (2004). Mapping regional land cover with MODIS data for biological conservation: Examples form the Greater Yellowstone Ecosystem, USA and Pará State, Brazil. *Remote Sensing of Environment, 92*, 67-83

White, M., Hoffman, F., Hargrove, W., & Nemani, R.R. (2005). A global framework for monitoring phenological responses to climate change. *Geophysical Research Letters, 32*

Woods, W.I. (1995). Comments on the Black Earths of Amazonia. In F.A. Schoolmaster (Ed.), *Applied Geography Conferences* (pp. 159-165). Arlington, Virginia

Woods, W.I. (2003). History of anthrosol research. In J. Lehmann, D. Kern, B. Glaser & W.I. Woods (Eds.), *Amazonian Dark Earths: Origin, Properties, Management* (pp. 29-50). Netherlands: Kluwer Academic Publishers

Woods, W.I. & Denevan W.M. (2009). Amazonian Dark Earths: The first century of reports. In W.I. Woods, W.G. Teixeira, J. Lehmann, C. Steiner, A.M.G.A. Winkler-Prins & L. Rebellato (Eds.), *Amazonian Dark Earths: Wim Sombroek's Vision*. Springer

Woods, W.I., & McCann, J.M. (1999). The Anthropogenic Origin and Persistence of Amazonian Dark Earths. *Yearbook 1999 - Conference of Latin Americanist Geographers, 25*, 7-14

Woods, W.I., McCann, J.M., & Meyer, D.W. (2000). Amazonian Dark Earth Analysis: State of Knowledge and Directions for Future Research. In F.A. Schoolmaster (Ed.), *Applied Geography Conferences* (pp. 114-121). Tampa, Florida

Wright, S., & Van Schaik, C. (1994). Light and phenology of tropical trees. *The American Naturalist, 143*, 192-199

Xiao, X., Hagen, S., Zhang, Q., Keller, M.E., & Moore, B.I. (2006). Detecting leaf phenology of seasonally moist tropical forests in South America with multi-temporal MODIS images. *Remote Sensing of Environment, 103*, 465-473

Xiao, X., Zhang, Q., Saleska, S., Hutyra, L., De Camargo, P., Wofsy, S.C., Frolking, S., Boles, S., Keller, M.E., & Morre III, B. (2005). Satellite-based modeling of gross primary production in a seasonally moist tropical evergreen forest. *Remote Sensing of Environment, 94*, 105-122

Zhang, X., Friedl, M.A., Schaaf, C.B., Strahler, A.H., Hodges, J.C., Gao, F., Reed, B.C., & Huete, A. (2003). Monitoring vegetation phenology using MODIS. *Remote Sensing of Environment, 84*, 471-475

Zimmerman, J.K., Wright, S.J., Calderón, O., Pagan, M.A., & Paton, S. (2007). Flowering and fruiting phenologies of seasonal and aseasonal neotropical forests: the role of annual changes in irradiance. *Journal of Tropical Ecology, 23*, 231-251